Running Title: Immunity-and-Matrix-Regulatory Cells Derived from hESCs…

Immunity-and-Matrix-Regulatory Cells Derived from Human Embryonic Stem Cells Safely and Effectively Treat Mouse Lung Injury and Fibrosis

Jun Wu[1,2,3,16], Dingyun Song[6,7,16], Zhongwen Li[1,2,3,16], Baojie Guo[1,2,3,4,16], Yani Xiao[11], Wenjing Liu[1,2,3], Lingmin Liang[1,2,3], Chunjing Feng[1], Tingting Gao[1,2,3], Yanxia Chen[1,2,3], Ying Li[15], Zai Wang[8], Jianyan Wen[8,9], Shengnan Yang[6,10], Peipei Liu[6,7], Lei Wang[1,2,3], Yukai Wang[1,2,3], Liang Peng[8], Glyn Nigel Stacey[3,5], Zheng Hu[13,14], Guihai Feng[1,2], Wei Li[1,2], Yan Huo[11], Ronghua Jin[12], Ng Shyh-Chang[1,2,4], Qi Zhou[1,2,3,4], Liu Wang[1,2,3,4], Baoyang Hu[1,2,3,4,*], Huaping Dai[6,7,*] and Jie Hao[1,2,3,*]

[1] State Key Laboratory of Stem Cell and Reproductive Biology, Institute of Zoology, Chinese Academy of Sciences, Beijing 100101, China

[2] Institute for Stem Cell and Regeneration, Chinese Academy of Sciences, Beijing 100101, China

[3] National Stem Cell Resource Center, Chinese Academy of Sciences, Beijing 100101, China

[4] University of Chinese Academy of Sciences, Beijing 100049, China

[5] International Stem Cell Banking Initiative, 2 High Street, Barley, Hertfordshire, SG8 8HZ, UK

[6] Department of Pulmonary and Critical Care Medicine, Center of Respiratory Medicine, China-Japan Friendship Hospital; National Clinical Research Center for Respiratory Diseases, Institute of Respiratory Medicine, Chinese Academy of Medical Sciences; Beijing 100029, China

[7] Graduate School of Peking Union Medical College, Chinese Academy of Medical Science and Peking Union Medical College, Beijing 100730, China

[8] Institute of Clinical Medical Sciences, Center of Respiratory Medicine, China-Japan Friendship Hospital, Beijing, China; Institute of Respiratory Medicine, Chinese Academy of Medical

Sciences, Beijing 100029, China

[9] Department of Cardiology, China-Japan Friendship Hospital; Beijing 100029, China

[10] Medical University of Ha Er Bin, Heilong Jiang Province, Ha Er Bin 150081, China

[11] National Center for Safety Evaluation of Drugs, National Institutes for Food and Drug Control, Beijing 100176, China

[12] Beijing Youan Hospital, Capital Medical University, Beijing 100069, China

[13] Key Laboratory of Organ Regeneration & Transplantation of Ministry of Education, The First Hospital of Jilin University, Changchun 130061, China

[14] National-Local Joint Engineering Laboratory of Animal Models for Human Diseases, Changchun 130061, China

[15] Department of Gastroenterology, The First Hospital of Jilin University, Changchun, 130061, China

[16] These authors contributed equally.

*Correspondence: haojie@ioz.ac.cn, byhu@ioz.ac.cn, daihuaping@ccmu.edu.cn

Abstract

Lung injury and fibrosis represent the most significant outcomes of severe and acute lung disorders, including COVID-19. However, there are still no effective drugs to treat lung injury and fibrosis. In this study, we report the generation of clinical-grade human embryonic stem cells (hESCs)-derived immunity- and matrix-regulatory cells (IMRCs) produced under good manufacturing practice (GMP) requirements, that can treat lung injury and fibrosis in vivo. We generate IMRCs by sequentially differentiating hESCs with serum-free reagents. IMRCs possess a unique gene expression profile distinct from umbilical cord mesenchymal stem cells (UCMSCs), such as higher levels of proliferative, immunomodulatory and anti-fibrotic genes. Moreover, intravenous delivery of IMRCs inhibits both pulmonary inflammation and fibrosis in mouse models of lung injury, and significantly improves the survival rate of the recipient mice in a dose-dependent manner, likely through paracrine regulatory mechanisms. IMRCs are superior to both primary UCMSCs and FDA-approved pirfenidone, with an

excellent efficacy and safety profile in mice and monkeys. In light of public health crises involving pneumonia, acute lung injury (ALI) and acute respiratory distress syndrome (ARDS), our findings suggest that IMRCs are ready for clinical trials on lung disorders.

Introduction

Lung injury is a serious threat to human health. It is caused by many chemical, physical and biological agents, resulting in pneumonia, lung inflammation, and fibrosis. In a comprehensive analysis, the World Health Organization ranks lung diseases as the second largest category, and predicts that by 2020, about one fifth of human deaths will be attributed to lung diseases[1]. Acute lung injury (ALI) is the injury of alveolar epithelial cells and capillary endothelial cells caused by various direct and indirect injury factors, resulting in diffuse pulmonary interstitial and alveolar edema, and acute hypoxic respiratory insufficiency. Pathophysiologically, its characteristics include decreased lung volume, decreased lung extensibility and imbalance of the ventilation/blood flow ratio. When ALI develops into the severe stage (oxygenation index < 200), it is called acute respiratory distress syndrome (ARDS). Globally, there are more than 3 million patients with ARDS annually, accounting for 10% of intensive care unit (ICU) admissions[2]. ALI/ARDS patients have an average mortality rate of 35-46%[3,4]. In late ARDS, pulmonary fibrosis (PF) develops due to persistent alveolar injury, repeated destruction, repair, reconstruction and over-deposition of extracellular matrix (ECM)[5], leading to progressive lung scars and common interstitial pneumonia. In general, idiopathic pulmonary fibrosis (IPF) patients show very poor prognosis, with a median survival time of 3-5 years after diagnosis[6]. It has also been reported that the degree of pulmonary fibrosis is closely related to the mortality of ARDS[7,8]. Importantly, there are still no effective FDA-approved drugs to treat ALI, ARDS or IPF hitherto, and most experimental drugs are still in the midst of Phase II or Phase III clinical studies[2, 9,10].

Stem cell therapy is an emerging treatment modality being used to cure various inflammatory and/or degenerative diseases, including ALI and PF. In particular, mesenchymal stem cells (MSCs) have been tested as an intravenous infusion therapy for ALI and PF[11,12]. Preclinical and clinical studies of pulmonary fibrosis have shown that, after infusion, MSCs could migrate to the sites of lung injury, inhibit inflammation and improve recovery[13-15]. However, clinical studies with primary MSCs derived from the umbilical cord, bone marrow or adipose tissue have been hampered by the lack of available

82 donors, limited cell numbers from each donor, donor and tissue heterogeneity, inconsistent cell quality
83 and the lack of standardized cell preparations. Moreover, primary MSCs show limited self-renewal
84 capacities and finite lifespans. MSC-like cells derived from human embryonic stem (hESCs)[16] could
85 solve these problems[17-19], but the use of ill-defined and variable components of animal origin, such as
86 fetal bovine serum (FBS) or OP9 feeder cells, may greatly compromise their consistency, safety and
87 clinical applicability. Furthermore, these hESC-derived MSC-like cells have not been deeply
88 characterized for their immunomodulatory functions in disease models.
89 In this study, we demonstrate that our hESC-derived MSC-like cell population have unique abilities in
90 modulating the immunity and regulating extracellular matrix production, compared to regular MSC
91 populations. Therefore, we named it as immunity- and matrix-regulatory cells (IMRCs). One aspect of
92 IMRCs is that they resemble MSCs in their capacity for self-renewal and tri-lineage differentiation.
93 However, compared to primary umbilical cord mesenchymal stem cells (UCMSCs), IMRCs also
94 displayed a higher consistency in quality, stronger immunomodulatory and anti-fibrotic functions, and
95 a robust ability to treat lung injury and fibrosis in vivo.

96 **Materials and methods**

97 **Generation of hESC-derived IMRCs**

98 The hESC-derived IMRCs were generated by passaging cells that are migrating out from human
99 embryoid bodies (hEBs), with serum-free reagents. The clinical hESC line (Q-CTS-hESC-2) was
100 prepared as described previously[20]. Clinical hESCs were maintained in commercially available
101 Essential 8™ (E8) basal medium (Gibco, Carlsbad, MO, USA; A15169-01) with Essential 8™
102 Supplement (Gibco, A15171-01) on vitronectin-coated plates (1 μg/cm^2). To generate embryoid bodies
103 (hEBs), hESCs were dissociated into small clumps by incubating at 37 °C for 5 min with 1 mg/mL
104 dispase (Gibco, 17105-04) and cultured to form hEBs for 5 days in KO-DMEM (Gibco, A12861-01)
105 supplemented with 20% KOSR (Gibco, A3020902), 1 × L-glutamine (Gibco, A12860-01), 1 × NEAA
106 (Gibco, 11140050) and 10 ng/mL bFGF (Thermo, 13256029). Then, hEBs were transferred onto
107 vitronectin-coated plates and cultured for 14 additional days. During this period, the outgrowth from
108 the hEBs occurred. The outgrowth cells were dissociated by using Tryple (Gibco, A12859-01) and
109 passaged at a low cell density of 1 × 10^4 cells per cm^2 in "IMRCs Medium" consisting of α-MEM

110 (Gibco, 12561-049) supplemented with 5% KOSR, 1% Ultroser G (Pall corporation, New York, NY,
111 USA; 15950-017), 1 × L-glutamine, 1 × NEAA, 5 ng/mL bFGF and 5 ng/mL TGF-β (Peprotech,
112 96-100-21-10). Cells were passaged upon reaching approximately 80% confluence in IMRCs Medium.
113 After 5 passages in culture, differentiated cultures were harvested for characterization. By this time,
114 IMRCs displayed a fibroblastic morphology, expressed canonical "MSC-specific" surface markers
115 including CD73, CD90, CD105 and CD29 and were negative for typical hematopoietic markers (CD45,
116 CD34, HLA-DR)[21,22].

117 **Isolation and culture of UCMSCs**

118 Healthy full-term human placental samples were collected according to the policy of the Ethics
119 Committee of the 306th Hospital of the Chinese People's Liberation Army, Beijing, China. Written
120 informed consents were obtained from all donors before this study. All the samples were used in
121 accordance with standard experimental protocols approved by the Animal and Medical Ethical
122 Committee of Institute of Zoology, Chinese Academy of Sciences, Beijing, China.

123 Briefly, the newborn umbilical cords of full-term pregnancies were obtained from the clinic and
124 washed by PBS to remove all remnant blood. Then, the umbilical cords were cut to approximately 2
125 mm in size after removing the artery and vein. The pieces of umbilical cords were directly transferred
126 into a 10 cm^2 culture flasks in α-MEM supplemented with 5% KOSR, 1% Ultroser G, 1 × L-glutamine,
127 1 × NEAA and 5 ng/mL bFGF, and cultured in an atmosphere of 5% CO_2 at 37 °C. UCMSCs were
128 passaged upon reaching approximately 80% confluence. After 5 passages in culture, cells were
129 harvested for characterization.

130 **Cell culture**

131 The clinical hESC line (Q-CTS-hESC-2) was prepared as described previously[20]. Clinical hESCs were
132 maintained in the commercially available Essential 8™ (E8) basal medium on vitronectin-coated plates.
133 Cells were passaged every 5 or 6 days using Versene (Gibco, A4239101). Clinical hESCs were tested
134 weekly for mycoplasma contamination using a Myco-detection Kit (InvivoGen, San Diego, CA, USA;
135 rep-pt1) and endotoxin contamination was tested using a ToxinSensor™ Chromogenic LAL Endotoxin
136 Assay Kit (GenScript, Piscataway, NJ, USA; L00350). All cultures were maintained at 37 °C, 5% CO_2

137 and atmospheric O_2 in a humidified incubator (Thermo Fisher Scientific, Waltham, MA, USA). A549
138 cells were purchased from Beina Biology (Shanghai, China). The cells were cultured in Ham's F-12K
139 medium (Gibco, 21127022) with 10% fetal bovine serum (FBS; Gibco, 10091-148) at 37 °C in 5%
140 CO_2, and were treated with 10 ng/mL TGF-β1 (R&D systems, 240-B) or IMRC conditioned medium
141 where specified. To prepare the conditioned medium of IMRCs, IMRCs were cultured to 50%
142 confluence in culture dishes, then, were changed to new medium. The conditioned medium was
143 harvested after incubating IMRCs for 24 h.

144 **Karyotyping**

145 At passage 5, IMRCs were harvested. Karyotype analysis and G-binding were conducted at the
146 Chinese Academy of Medical Science & Peking Union Medical College (Beijing, China).

147 **RNA-seq library preparation and data analysis**

148 Total RNA was isolated from hESCs, IMRCs and UCMSCs by Trizol (Invitrogen, Waltham, MA,
149 USA; 15596018). RNA-seq libraries were prepared with the NEBNext®Ultra™ RNA Library Prep Kit
150 for Illumina®. Sequencing was performed on an Illumina HiSeq X-Ten sequencer with 150 bp
151 paired-end sequencing reaction. The bulk RNA-Seq data for hESCs were downloaded from GEO
152 database[23]. All RNA-sequencing data analysis was performed with Hisat2 (version 2.1.0)[24] and
153 Cufflinks (version 2.2.1)[25] using the UCSC hg19 annotation with default settings. Reads with unique
154 genome locations and genes with no less than 1 FPKM in at least one sample were used for the next
155 step of analysis. Two-fold change was used as the threshold to filter for differentially expressed genes
156 (DEGs) i.e. increased or decreased expression of less than 2-fold was not considered significant. The
157 Gene Ontology analysis for differentially expressed genes was performed by DAVID (version 6.8)[26].
158 Clustering, heatmap, Venn diagram and scatterplots analysis were performed with hierarchical cluster
159 and heatmap.2 functions in R. Pearson correlation coefficient was calculated by cor.test in R. Gene set
160 enrichment analysis were performed by GSEA[27].

161 **Flow cytometry**

162 Cells were harvested and blocked with 2% bovine serum albumin (BSA; Sigma-Aldrich, B2064) for 20
163 min at room temperature. Then, the cells were stained with fluorescein-conjugated antibodies for 40
164 min at room temperature in 1% BSA. After incubation, cells were washed 3 times and analyzed with
165 MoFlo (Beckman, Brea, CA, USA) and associated software. The antibodies used for flow cytometry
166 were as follows: PE-conjugated mouse anti-human CD29 (Biolegend, San Diego, CA, USA; 303004),
167 PE-conjugated mouse anti-human CD73 (BD Biosciences, San Jose, CA, USA; 550257),
168 PE-conjugated mouse anti-human CD90 (eBioscience, San Diego, CA, USA; 12-0909-42),
169 PE-conjugated mouse anti-human CD105 (Biolegend, 323206), PE-conjugated mouse anti-human
170 CD34 (BD Biosciences, 555822), PE-conjugated mouse anti-human CD45 (BD Biosciences, 560957),
171 PE-conjugated mouse anti-human HLA-DR (BD Biosciences, 555561), and the PE-conjugated mouse
172 IgG1 (BD Biosciences, 551436) as an isotype control.

173 **Trilineage differentiation**

174 Osteogenic, adipogenic, and chondrogenic differentiation experiments were performed following the
175 instructions of the human mesenchymal stem cell functional identification kit (R&D systems, SC006).
176 For osteogenic differentiation, 4.2×10^3 cells were seeded per well in 96-well plates. When cells
177 reached 50-70% confluency, the medium was replaced with osteogenic differentiation medium and
178 kept for 3 weeks. To assess osteogenic differentiation, immunofluorescence (Osteocalcin) and Alizarin
179 Red S (Sigma-Aldrich, A5533) staining was performed for the calcium-rich extracellular matrix. For
180 adipogenic differentiation, cells were seeded into a 24-well plate at the density of 3.7×10^4 cells/well,
181 and maintained in culture medium until 100% confluency. Then, cells were cultured in adipogenic
182 differentiation medium for 3 weeks. Lipid droplets of the resultant differentiated cells were detected
183 using immunofluorescence (FABP-4) and Oil red O (Sigma-Aldrich, O0625) staining. For
184 chondrogenic differentiation, 2.5×10^5 cells resuspended in chondrogenic differentiation medium were
185 centrifuged for 5 min at 200 g in a 15-mL conical tube (Corning, NY, USA). Then, cells were cultured
186 for 3 weeks. After 3 weeks, chondrogenic pellet was harvested and fixed in 4% paraformaldehyde
187 (Aladdin Chemical Co., Ltd., Shanghai, China; C104190). Cryosectioning was performed by OTF
188 Cryostat (Leica, Germany) and 10 μm sections were stained with immunofluorescence (Aggrecan) and
189 Alcian Blue (Sigma-Aldrich, A5268) staining.

190 **Growth curve**

191 IMRCs and UCMSCs were seeded into 96-well plates at a density of 8 × 10^3 cells per well. Cell
192 Counting Kit-8 (CCK8; Thermo Fisher Scientific, CK04) was used to measure the cells' growth. CCK8
193 solution was added at day 1, day 3, day 5 and day 7 by following the CCK8 kit manufacturer's protocol.
194 After 2 h of incubation, absorbance was measured at 450 nm.

195 **Cell diameter analysis**

196 The IMRCs and UCMSCs were harvested at passage 5 and the cell diameters were measured with
197 Image J software (NIH) software analysis. Normal Distribution curves were fitted to the cell diameter
198 data to analyze the cell size distribution characteristics.

199 **Cell viability test**

200 The IMRCs and UCMSCs were cryopreserved in a published clinical injection[28] for 15 days in liquid
201 nitrogen. After complete recovery of the cells, cells were suspended in clinical injection and remained
202 under 4 °C. Then, cell viability was determined using 0.4% (w/v) Trypan Blue (Gibco, 15250061) at
203 different time points by a Cell Counter (Invitrogen, Countess II) using the average of 3 replicates.

204 **Single-cell RNA-seq library preparation & sequencing**

205 IMRCs and UCMSCs were harvested and suspended in PBS. Then, cell suspensions were loaded onto
206 the Chromium Single Cell Controller (10 × Genomics) to generate single Gel Beads-in-Emulsion
207 (GEMs) by using Single Cell 30 Library and Gel Bead Kit V2 (10 × Genomics, 120237). Cells were
208 lysed and the released RNA was barcoded through reverse transcription in individual GEMs. Following
209 reverse transcription, cDNAs with both barcodes were amplified, and a library was constructed using
210 the Single Cell 30 Reagent Kit (v2 chemistry) for each sample following the manufacture's
211 introduction (performed by CapitalBio Technology, Beijing). Sequencing was performed on an
212 Illumina NovaSeq 6000 System in the 2 × 150 bp paired-end mode. Raw files were processed with Cell
213 Ranger using default mapping arguments. Gene expression analysis and cell type identification were
214 performed by Seurat V3.1. Briefly, after normalizing and quality control, the tSNE was used for

215 non-linear dimensional reduction. The figures were produced by DimPlot and VlnPlot functions in
216 Seurat.

217 **Cell culture with IFN-γ treatment**

218 Cells at passage 4 were digested and seeded into 6-well plates. IMRCs were seeded at a density of 3 ×
219 10^5 cells/well, and UCMSCs were seeded at a density of 2 × 10^5 cells/well. After adherence for 24 h,
220 IFN-γ (0, 25, 50, 100 ng/mL) (R&D systems, 285-IF) was added into the culture medium to culture for
221 24 h. Cells and conditioned medium were harvested after IFN-γ stimulation for qPCR and cytokine
222 analysis.

223 **Cytokine analysis**

224 Conditioned medium of UCMSCs and IMRCs were collected after IFN-γ (100 ng/mL) stimulation for
225 24 h. Forty-eight cytokines including FGF basic, Eotaxin (also known as CCL11), G-CSF (CSF3),
226 GMCSF (CSF2), IFN-γ, IL-1β, IL-1RA, IL-2, IL-4, IL-5, IL-6, IL-7, IL-8 (also known as CXCL8),
227 IL-9, IL-10, IL-12 (p70), IL-13, IL-15, IL-17α, IP10 (CXCL10), MCP1 (CCL2), MIP-1α (CCL3),
228 MIP-1β (CCL4), PDGFB, RANTES (CCL5), TNF-α, VEGF, IL-1α, IL-2Rα, IL-3, IL-12 (p40), IL-16,
229 GRO-α, HGF, IFN-α2, LIF, MCP-3, MIG, β-NGF, SCF, SCGF-β, SDF-1α, CTACK, MIF, TRAIL,
230 IL-18, M-CSF, TNF-β were detected by using the premixed 48-plex Bio-Plex Pro Human Cytokine
231 Assay (Bio-Rad, Hercules, CA, USA; 12007283) according to the manufacturer's instructions.

232 **Lymphocyte proliferation assay**

233 For the proliferation analysis, peripheral blood mononuclear cells (PBMCs) from umbilical cord blood
234 of healthy donors were stimulated by 5 μg/mL phytohaemagglutinin (PHA; Sigma-Aldrich, L4144) in
235 a 96-well plate for 3 days in the presence or absence of IMRCs (2 × 10^5/well) at a ratio of 1:1. At day 3,
236 the proliferation of PBMCs was analyzed by CCK8.

237 **Real-time quantitative PCR**

238 For reverse transcription (RT), RNA was extracted using an RNAprep Pure Cell/Bacteria Kit
239 (TIANGEN, Beijing, China; DP430). Two micrograms of RNA were reverse transcribed into cDNA

240 using a PrimeScript™ First-Strand cDNA Synthesis Kit (TaKaRa, Shiga, Japan; 6110B). Real-time
241 quantitative PCR (qPCR) was performed and analyzed using a Stratagene Mx3005P system (Agilent
242 Technologies, Santa Clara, CA, USA) with SYBR Green Real-Time PCR Master Mix Plus (Toyobo,
243 Osaka, Japan; QPS-201). *GAPDH* was used for internal normalization. Primers for real-time PCR in
244 this study are as shown in Supplementary information, Table S2.

245 **Enzyme-linked immunosorbent assay (ELISA)**

246 To determine the secretion of human MMP1, cell culture supernatants were collected after 48 hours of
247 culture. The levels of human MMP1 protein were measured by a Human MMP1 ELISA Kit (Cusabio,
248 Wuhan, China; CSB-E04672h) according to the manufacturer's instructions. Concentrations of TNF-α
249 (Expandbio, Beijing, China; Exp210030) and TGF-β1 (Expandbio, Exp210089) in the mouse lung
250 homogenates were measured using ELISA kits according to the manufacturer's instructions.

251 **Human MMP1 activity**

252 To determine the activity of human MMP1, cell culture supernatants were collected after 48 hours of
253 culture. The activity of human MMP1 were measured by a SensoLyte® Plus 520 MMP-1 Assay Kit
254 (AnaSpec, San Jose, CA, USA; AS-72012) according to the manufacturer's instructions. A specific
255 anti-MMP-1 monoclonal antibody was used in combination with an MMP1 fluorogenic substrate,
256 5-FAM/QXL®520 FRET peptide. The fluorescence signal is monitored at Ex/Em = 490 nm/520 nm
257 upon MMP-1-induced cleavage of the FRET substrate.

258 **Immunofluorescence staining**

259 Cells were fixed with 4% paraformaldehyde for 15 min, permeabilized with 0.5% Triton X-100 for 15
260 min and blocked with 2% BSA for 60 min at room temperature. Then, the cells were stained with 1:200
261 mouse monoclonal IgG E-cadherin (Abcam, San Francisco, CA, USA; ab1416), 1:200 rabbit
262 monoclonal IgG Collagen I (Cell Signaling Technology, Danvers, MA, USA; 84336), 1:200 rabbit
263 anti-FABP-4 (Thermo Fisher Scientific, PA5-30591), 1:200 rabbit anti-Osteocalcin (Thermo Fisher
264 Scientific, PA5-11849), 1:200 mouse anti Aggrecan (Thermo Fisher Scientific, MA3-16888) overnight
265 at 4 °C in 2% BSA in PBS. The cells were washed 3 times with PBS and then incubated with 1:200
266 Alexa Fluor 488 donkey anti-mouse IgG (H+L) (Jackson ImmunoResearch, West Grove, PA, USA;

267 715-545-151), 1:200 Fluorescein (Cy3) donkey anti-rabbit IgG (H + L) (Jackson ImmunoResearch,
268 711-165-152), 1:200 Fluorescein (Cy3) donkey anti-mouse IgG (H + L) (Jackson ImmunoResearch,
269 715-165-151) or Fluorescein (Cy2) donkey anti-rabbit IgG (H + L) (Jackson ImmunoResearch,
270 711-545-152) secondary antibodies in 2% BSA for 60 min at room temperature in the dark. The
271 washing step was repeated before staining the nuclei with Hoechst 33342 (Invitrogen, H3570).

272 **Western blot**

273 Cells were harvested in RIPA Lysis Buffer (strong) (CWbio, Taizhou, China; CW2333S) containing
274 protease inhibitors (Roche, 4693124001). A total of 40 μg proteins were separated by 4-20% gradient
275 SDS-PAGE gels (GenScript, M42015C) and transferred to PVDF membranes (Millipore, Billerica,
276 MA, USA; IPVH00010). The membranes were blocked at room temperature with 1% BSA for 1 h and
277 incubated overnight at 4 °C with primary antibodies: rabbit Collagen I antibody (Cell Signaling
278 Technology, 84336), mouse E-cadherin antibody (Abcam, ab1416), mouse α-SMA antibody
279 (Sigma-Aldrich, A5228) and mouse β-actin antibody (Sigma-Aldrich, A1978). Then, the membranes
280 were washed with TBST for 3 times and incubated for 1 h with a secondary antibody: anti-mouse IgG
281 antibody (HRD) (Sigma-Aldrich, A9044) and anti-rabbit IgG antibody (HRD) (Sigma-Aldrich, A0545)
282 at room temperature. Images were obtained using the ChemiDoc XRS+ imaging system (Bio-Rad) and
283 quantified using the Quantity One software.

284 **Soft agar colony formation assay**

285 Soft agarose gels were prepared according to previously published protocols[29]. Cells were harvested
286 and diluted to a cell concentration of 2.5×10^4 cells/mL, before mixing with the agarose mixture in
287 6-well culture plates. The plates were incubated in a 37 °C incubator for 21 days.

288 **Animals**

289 Adult female and male cynomolgus monkeys (3-5 years old) were housed in single quarters with a
290 12/12 h light/dark cycle. Animals were provided with monkey chow and enrichment food twice a day
291 and water *ad libitum*. The monkey experiments were performed at the National Center for Safety
292 Evaluation of Drugs, National Institutes of Food and Drug Control (Beijing, China). The Institutional

293 Animal Care and Use Committee of the National Center for Safety Evaluation of Drugs approved all
294 monkey studies (NO. IACUC-2018-k001).
295 Specific pathogen-free (SPF) 11- to 13-week-old C57BL/6 male mice were purchased from the Animal
296 Center of Peking University (Beijing, China). All experimental and control mice were weight-matched,
297 and their weights ranged from 25 to 30 g. All mice were housed in the animal care facility of the
298 Institute of Medical Science, China-Japan Friendship Hospital. Mice were maintained under SPF
299 conditions at room temperature (between 20-24 °C), with humidity between 35-55%, in a 12/12 h
300 light/dark cycle, with food and water *ad libitum* and monitored with respect to their general state, fur
301 condition, activity, and weight according to institutional guidelines. The mice were sacrificed at each
302 observational time point by using intraperitoneal pentobarbital overdose. The Animal Studies
303 Committee of the China-Japan Friendship Hospital (Beijing, China) approved all mice studies
304 (NO.190108).

305 **Acute toxicity and long-term toxicity test**

306 Acute toxicity test: Low dose (2.6×10^6 cells/monkey), middle dose (2.6×10^7 cells/monkey) and high
307 dose (1×10^8 cells/monkey) IMRCs were infused into cynomolgus monkeys (3-5 years old) by single
308 intravenous infusion. After 6 months, their body weight, ophthalmology status, hematology, blood
309 chemistry and urine chemistry were measured.
310 Long-term toxicity test: Low dose (2.6×10^6 cells/monkey) and high dose (1×10^8 cells/monkey)
311 IMRCs, or saline, were injected into cynomolgus monkeys (3-5 years old) by intravenous infusion once
312 a week for 22 times, after which their body weight, body temperature, food intake and organ weights
313 were measured.

314 **Copy number variation calling**

315 30X whole-genome sequencing data was produced by HiSeq X-Ten (Annoroad Gene Technology Co.,
316 Ltd) and used to analyze single nucleotide mutation changes between IMRCs and hESCs. As
317 previously described[30], the whole-genome sequencing data was mapped to the hg19 reference genome
318 by BWA (version 0.7.15) using the 'mem' mode with default parameters. The genome coverage was
319 calculated by bedtools[31]. The normalized coverage depth for each bin was calculated by dividing the

raw coverage depth by the average sequencing depth. Duplicate reads were removed and the uniquely mapped reads were retained for the copy-number variation (CNV) analysis, in which chromosomal sequences were placed into bins of 500 kb in length. The hg19 genome repeat regions annotated by RepeatMasker (http://www.repeatmasker.org) were removed from the genomic sequence before calculating the coverage. The CNV scatterplot was drawn using ggplot2.

Histological staining and immunostaining staining analysis

Mouse lung histology was performed as follows. Briefly, the lung was dehydrated, paraffin-embedded and cut into 4 μm sections. Lung sections were stained with H&E and Masson's trichrome stain for assessment of pathological changes. Immunohistochemical staining was performed using antibodies against α-SMA (Servicebio, Wuhan, China; GB13044), Fibronectin (Servicebio, GB13091), Collagen I (Servicebio, GB13091) and GFP (Servicebio, GB13227). Immunofluorescence staining was performed using antibodies against GFP (Servicebio, GB13227), CD31 (Servicebio, GB11063-3) and SPC (Millipore, AB3786).

Labeling IMRCs with DiR dye

IMRCs were labeled with a lipophilic, near-infrared fluorescent dye 1,1-dioctadecyl-3,3,3,3-tetramethyl indotricarbocyanine iodide (DiR; YEASEN, Shanghai, China; 40757ES25). IMRCs were suspended at a concentration of 1×10^6 cells/mL and incubated with DiR buffer for 20 min at 37 °C according to the manufacturer's protocol. After incubation, cells were centrifuged at 1000-1500 rpm for 5 min. After washing twice with PBS and resuspension, the IMRCs were preheated at 37 °C before infusion. Both DiR-labeled and unlabeled cells (5×10^6 cells in 200 μL saline) were injected via the tail vein.

In vivo imaging of IMRCs' biodistribution

Mice were lightly anesthetized and were monitored using the in vivo imaging systems at day 0, day 1, day 3, day 5, day 7, day 9, day 15, day 21, day 27, day 32, day 37 and day 46 after tail intravenous injection of DiR-labeled IMRCs (5×10^6 cells in 200 μL saline). Serial fluorescence images were also obtained in major organs ex vivo. In order to reduce autofluorescence, the ideal filter conditions for

346 DiR imaging were an excitation/emission spectrum in the near infrared range (750/780 nm)[32,33].

347 **Lung function**

348 The flexiVentFX experimental platform was set up according to the manufacturer's instructions. At the
349 day 21, after 3% pentobarbital sodium (40 mg/kg) intraperitoneal injection of anesthesia, mice were
350 fixed supine within 5-8 minutes, and endotracheal intubation was inserted in the middle of a
351 tracheotomy. After computer processing, indicators of lung function required were obtained, including
352 the inspiratory capacity (IC), respiratory resistance (Rrs), static compliance (Crs), elastic resistance
353 (Ers), Newtonian resistance, tissue damping (G), tissue elasticity (H) and forced vital capacity (FVC)[34].

354 **Lung coefficient**

355 The lung tissue was completely removed, weighed by electronic balance, and the lung coefficient was
356 calculated according to the formula: wet lung weight (g)/total body weight (kg).

357 **Cell therapy in BLM mouse model of pulmonary fibrosis**

358 The BLM mouse model was generated by intratracheal injection of 1.5 $mg \cdot kg^{-1}$ bleomycin sulphate
359 (BLM; Bioway, China; DP721) in normal saline under light anaesthesia. The IMRCs were delivered
360 intravenously at day 0 or day 1 or day 7 or day 14 after injury. Mice were euthanized with 50 mg/mL
361 sodium pentobarbital (0.6 mg/10 g weight) according to published guidelines[35]. Animals were killed at
362 day 21 after BLM injury. After perfusion with normal saline, the left lungs were used for morphometric
363 analysis while the right lungs were removed and used for other analyses.

364 **Micro-CT**

365 Mouse CT scans were performed according to the manufacturer's instructions.

366 **Compassionate use study of two severely ill COVID-19 patients**

367 We conducted a pilot study using GMP-grade IMRCs, under an expanded access program for
368 compassionate use in COVID-19 patients. The pilot study was approved by the Ethics Committee of
369 the Beijing Youan Hospital, Capital Medical University (LL-2020-010-K, Youan EC [2020]005). After

370 two severely ill COVID-19 patients, who tested positive for SARS-CoV-2 by qPCR and were
371 diagnosed with ALI (aged 44-46 years; 1 male and 1 female), gave their consent and met the eligibility
372 criteria, their serum samples were collected and processed in accordance with the ethical legislation
373 and the guidelines of the Ethics Committee of the Beijing Youan Hospital, Capital Medical University.

374 **Statistics**

375 All data are expressed as mean ± SEM. Survival curves were derived by the Kaplan-Meier method and
376 compared via generalized Wilcoxon test. Statistical analysis was performed using GraphPad Prism 5.0
377 statistical software (San Diego, CA, USA). The statistical significance of multiple groups was
378 compared to each other using Tukey's multiple comparison test ANOVA. A p value of < 0.05 was
379 considered statistically significant.

380

381 **Results**

382 **Generation of hESC-derived IMRCs**

383 In this study, hESC-derived IMRCs were generated by passaging cells that are migrating from human
384 embryoid bodies (hEBs), using serum-free reagents (Fig. 1a, b). The clinical hESC line
385 (Q-CTS-hESC-2) was prepared as described previously[20]. Clinical hESCs were maintained in Essential
386 8™ basal medium (E8) on vitronectin-coated plates, before dissociation into small clumps to form
387 hEBs for 5 days. Subsequently, hEBs were transferred onto vitronectin-coated plates and cultured for
388 14 additional days. The hEBs outgrowth cells were dissociated and passaged continuously in IMRCs
389 Medium. After 5 passages, IMRCs were harvested for characterization. IMRCs possessed
390 fibroblast-like morphology (Fig. 1b) and maintained diploid karyotypes at passage 5 (Fig. 1c).
391 Moreover, copy-number variation analysis by whole genome sequencing data also indicated that no
392 chromosomal aneuploidies, large deletions nor duplication fragments were detected (Fig. 1d). Next, we
393 analyzed the expression profile of MSC-specific genes (Fig. 1e). IMRCs showed a pattern that greatly
394 differed from hESCs, and closely resembled primary umbilical cord-derived MSCs (UCMSCs). All
395 pluripotency genes (*POU5F1*, *SOX2, NANOG, ZFP42, SALL4*), mesendoderm genes (*MIXL1*), and
396 ectoderm genes (*GAD1*) were extinguished in both IMRCs and UCMSCs (Fig. 1e). IMRCs expressed

397 MSC-specific genes, including *PDGFRA* and *SPARC,* and the MSC-specific surface markers *NT5E*
398 (CD73), *ENG* (CD90), *THY1* (CD105) and *ITGB1* (CD29). Flow cytometry analysis further confirmed
399 this surface marker profile (Fig. 1f; Supplementary information, Fig. S1a, b). By contrast, IMRCs were
400 negative for the hematopoietic surface markers *PTPRC* (CD45) and CD34. IMRCs displayed the
401 ability to undergo tri-lineage differentiation into mesenchymal tissues, such as adipocytes,
402 chondroblasts and osteoblasts (Fig. 1g; Supplementary information, Fig. S1c). The proliferation rate of
403 IMRCs was higher than that of UCMSCs at passage 15, suggesting that IMRCs have a stronger
404 capacity for long-term self-renewal than primary MSCs (Fig. 1h). Interestingly, IMRCs were generally
405 smaller than UCMSCs (Fig. 1i), suggesting that IMRCs can pass through small blood vessels and
406 capillaries more easily, and are thus perhaps less likely to cause pulmonary embolism. To evaluate the
407 clinical potential of the IMRCs, we measured the viability of IMRCs suspended in a published clinical
408 injection buffer at 4 °C. We found that the viability of IMRCs remained higher (93%) than UCMSCs
409 (73%) after 48h (Fig. 1j).

410 **IMRCs possess unique gene expression characteristics**

411 To clarify the degree of similarity between hESCs, IMRCs and primary UCMSCs at the whole
412 transcriptome level, we performed genome-wide profiling of IMRCs and UCMSCs and compared their
413 gene expression with hESCs[23]. Whole-transcriptome analysis confirmed that IMRCs clustered together
414 with UCMSCs in an unsupervised hierarchical clustering (Fig. 2a). The global differentially expressed
415 gene analysis showed that highly expressed genes in IMRCs and UCMSCs compared with hESCs,
416 were enriched with angiogenesis, inflammatory response and extracellular matrix disassembly related
417 processes (Supplementary information, Fig. S2). Accordingly, MSC-specific genes such as *NT5E, ENG,*
418 *PDGFRA, SPARC* and *ITGB1* were upregulated, whereas pluripotency genes such as *POU5F1, SOX2,*
419 *SALL4* and *ZFP42* were extinguished in IMRCs relative to hESCs, and the overall correlation with
420 hESCs was weak ($R^2 = 0.66$; Fig. 2b). Next, we analyzed the expression of genes specific to IMRCs,
421 compared to UCMSCs (Fig. 2c). While the overall correlation with UCMSCs was stronger ($R^2 = 0.87$),
422 we also found that many genes were differentially expressed in IMRCs compared to primary UCMSCs.
423 The upregulated genes promote immunomodulation (*LIF*), tissue repair (*VEGFA, GREM1*), cell
424 division (*CDC20*) and anti-fibrosis (*MMP1*). By contrast, the downregulated genes predominantly

425 promote inflammation (*IL-1B, CXCL8, CCL2* and *CXCL1;* Fig. 2c). Gene set enrichment analysis
426 (GSEA) of the differentially expressed genes confirmed that IMRCs manifest reduced inflammation
427 and stronger proliferative capacity as their top gene signatures, compared to primary UCMSCs (Fig. 2d,
428 e; Supplementary information, Fig. S3).
429 To elucidate the heterogeneity of gene expression amongst IMRCs, single cell RNA sequencing
430 (scRNAseq) was performed for both IMRCs and primary UCMSCs. A total of 16,000 single-cell
431 transcriptomes were obtained from two samples. Approximately ~ 100,000 reads were obtained per cell,
432 which generated a median of 31,000 unique molecular identifiers per cell, ~ 4,800 expressed genes per
433 cell and more than 22,000 total genes detected in the population. Our scRNAseq data also showed that
434 IMRCs were relatively homogenous in expression for the MSC-specific markers *PDGFRA, SPARC,*
435 *NT5E, ITGB1* and *ENG* (Fig. 2f; Supplementary information, Fig. S4). IMRCs were also relatively
436 homogenous in their suppression of pluripotency and non-mesenchymal markers, relative to hESCs
437 and UCMSCs, suggesting they are likely to be similar in biological activity to primary MSCs after
438 transplantation (Fig. 2g; Supplementary information, Fig. S4). These results provided insight into the
439 clinical applicability of IMRCs, especially with regards to their complete loss of pluripotency and their
440 gain in hyper-immunomodulatory potential.

441 **IMRCs treated with IFN-γ show hyper-immunomodulatory potency**

442 To test the immunomodulatory capacity of IMRCs, we exposed them to the pro-inflammatory cytokine
443 IFN-γ. We found that after stimulation with IFN-γ, both primary UCMSCs and IMRCs displayed
444 similar characteristic morphological changes (Fig. 3a). IFN-γ stimulation also potently upregulated
445 *IDO1* (indoleamine 2, 3-dioxygenase 1) expression in both primary UCMSCs and IMRCs, but much
446 more significantly so in IMRCs (Fig. 3b). This is important because *IDO1* has been shown to mediate
447 immunosuppression in T cell-inflamed microenvironments through its catabolism of tryptophan and
448 thus suppression of the tryptophan-kynurenine-aryl hydrocarbon receptor (Trp-Kyn-AhR) pathway in T
449 cells. To further characterize IMRCs at a molecular level, we conducted genome-wide RNA profiling
450 to compare IMRCs with UCMSCs, after IFN-γ stimulation (Fig. 3c). Hierarchical clustering revealed
451 that IMRCs clustered separately from UCMSCs, although they appeared more similar after IFN-γ
452 stimulation (Fig. 3d). To analyze IMRCs after IFN-γ stimulation in greater detail, we separated their

differentially expressed genes into different categories and tested their overlap using Venn diagram analysis (Fig. 3e). The global differential expressed gene analysis showed that highly expressed genes in IMRCs and UCMSCs after IFN-γ stimulation, compared with IMRCs and UCMSCs before IFN-γ stimulation, were enriched with immune response and interferon-gamma-mediated signaling pathway (Supplementary information, Fig. S5). Accordingly, we found that some pro-inflammatory genes showed lower expression while some pro-regenerative genes showed higher expression levels in IMRCs, compared to primary UCMSCs (Fig. 3f).

To confirm these findings, we performed a focused ELISA analysis of 48 biologically relevant chemokines and cytokines in the secretomes of both stimulated IMRCs and UCMSCs. We found that at least nine pro-inflammatory cytokines were lower in IMRCs than UCMSCs, including interleukin-6 (IL-6), IL-1β, tumor necrosis factor alpha (TNF-α), GRO-α, IFN-α2, IL-1α, IL-3, and IL-8 (Fig. 3g; Supplementary information, Fig. S6a). Furthermore, while the anti-inflammatory IL-4 was lower, the immunomodulatory cytokines IL-1RA, LIF, and RANTES were higher in IMRCs than UCMSCs (Fig. 3h). Amongst the pro-regenerative cytokines, we found that GM-CSF was similar while VEGFA, MIG and SDF-1α were higher in IMRCs than UCMSCs (Fig. 3i). To determine the immunomodulatory properties of IMRCs, we examined the effects of IMRCs on PBMCs' proliferation and found that IMRCs significantly inhibited PHA-stimulated PBMCs' proliferation when cocultured together at a ratio of 1:1 (Supplementary information, Fig. S6b). These results indicate that IMRCs manifest much stronger immunomodulatory and pro-regenerative functions than UCMSCs.

IMRCs suppress the pro-fibrotic effects of TGF-β1

Our scRNAseq results also indicated that more than 99% of IMRCs expressed *MMP1* compared with primary UCMSCs (< 1%) (Fig. 4a; Supplementary information, Fig. S4). Similarly, gene expression analysis by RT-qPCR showed that IMRCs express much higher levels of *MMP1* than hESCs, UCMSCs or human foreskin fibroblasts (HFF; Fig. 4b). MMP1 could be detected as a highly secreted protein in the conditioned media of IMRCs by ELISA (Fig. 4c). In addition, the secreted MMP1 was an enzymatically active and correctly processed isoform (Fig. 4d, e). To investigate the role of the IMRCs on fibrosis, the human epithelial cell line A549 was used to establish an in vitro fibrosis model. The morphology of A549 cells became myofibroblast-like after 48 h treatment with 10 ng/mL TGF-β1 (Fig.

481 4f). Consistent with the morphological changes, the expression of myofibroblast markers such as
482 *ACTA2*, *Collagen I*, *Collagen II*, *Fibronectin* and *TGFB1* increased, while the expression of the
483 epithelial identity marker *CDH1* was extinguished, suggesting that the A549 cells had undergone
484 TGF-β1-induced myofibroblast transdifferentiation (Fig. 4g). Immunofluorescence and western blot
485 analyses confirmed that TGF-β1 induced the upregulation of collagen I and the downregulation of
486 E-cadherin (Fig. 4h, i). These results indicated that the A549 alveolar epithelial cells could simulate
487 lung fibrosis in vitro. Thereafter, A549 cells were cultured with or without the conditioned media of
488 IMRCs, along with TGF-β1 treatment. Our results showed that the IMRC conditioned media
489 significantly ameliorated the induction of *Collagen I*, *ACTA2* and *TGFB1* expression (Fig. 4j;
490 Supplementary information, Fig. S7a). Immunofluorescence and western blot analyses further
491 confirmed that IMRC conditioned media could extinguish Collagen I protein expression and inhibit
492 α-SMA protein expression during the A549-to-myofibroblast transdifferentiation (Fig. 4k-m;
493 Supplementary information, Fig. S7b, c). These results suggested that IMRCs might be able to inhibit
494 lung fibrosis.

495 **Safety evaluation of IMRC transfusion into mice and monkeys**

496 Tumorigenicity has long been an obstacle to the clinical application of cells derived from hESCs, due
497 to the contamination of residual hESCs that could form teratomas. Our single cell RNA sequencing
498 showed that no residual $OCT4^{+}$/$SOX2^{+}$/$NANOG^{+}$/$TERT^{+}$/$DPPA5^{+}$ hESCs remained amongst the
499 IMRCs, and that all pluripotency gene expression had been extinguished (Fig. 5a). To ensure their
500 short-term and long-term safety, a series of biosafety-related experiments were performed according to
501 the "Guidelines for Human Somatic Cell Therapies and Quality Control of Cell-based Products" of
502 China Food and Drug Administration (CFDA) (http://samr.cfda.gov.cn/WS01/CL0237/15709.html),
503 whereupon the IMRCs were verified as suitable for use in human therapy (Supplementary information,
504 Table S1). These biosafety-related experiments included testing for bacteria, fungi, mycoplasma, virus
505 (by in vivo and in vitro methods), pluripotent cell residuals, tumorigenicity and biopreparation safety
506 (endotoxin and bovine serum albumin residuals). According to these tests, the safety of the IMRCs has
507 been verified as required by the National Institutes for Food and Drug Control (NIFDC) in China.
508 To track the biodistribution and long-term engraftment of IMRCs in vivo, whole-animal imaging of

509 wildtype mice was performed at designated time points (day 0, 1, 3, 5, 7, 9, 15, 21, 27, 32, 37 and 46)
510 after injection with DiR-labeled IMRCs (Supplementary information, Fig. S8a). Our data showed that
511 DiR fluorescence intensity declined by half on the 5th day, and dropped steadily over at least 15 days,
512 disappearing around day 46 (Fig. 5b, c; Supplementary information, Fig. S8c). No DiR fluorescence
513 signals were observed in the control mouse. These results indicate that IMRCs never show long-term
514 engraftment in vivo. However, IMRCs were predominantly distributed to the lung, with small amounts
515 in the liver and spleen (Supplementary information, Fig. S8b). To assess the recruitment of IMRCs to
516 the lung in greater detail, GFP-labeled IMRCs were used to track the distribution of IMRCs. A number
517 of GFP-labeled IMRCs were observed in the interstitial spaces in the lung, but not in the lung
518 capillaries (Fig. 5d). Immunofluorescence analysis of the expression of the alveolar type II epithelial
519 cell marker SPC and the endothelial cell marker CD31 showed that neither marker was co-expressed
520 with GFP-labeled IMRCs in the lungs of mice by day 21 (Fig. 5d). These data suggested that IMRCs
521 are unlikely to engraft nor transdifferentiate into endothelial or epithelial cells, after homing to the
522 interstitium of lung tissues in vivo.
523 To give some indication of the tumorigenic potential of IMRCs in vitro, a soft agar assay was
524 performed (Fig. 5e). As a positive control, the PANC-1 pancreas tumor cell line showed a colony
525 formation rate of about 30%. A small number of clones were also formed by hESCs, and the colony
526 formation rate was about 0.5%. However, no colonies were formed by IMRCs. These results indicated
527 that IMRCs had no tumorigenic potential as determined by this assay. Somatic mutation analysis by
528 whole genome sequencing also showed zero mutations in all coding and noncoding exon regions of the
529 IMRCs genome (Fig. 5f). Tumor formation assays also confirmed that IMRCs could not form any
530 tumors in immunodeficient mice after injection in vivo (Supplementary information, Table S1).
531 We also transfused different doses of IMRCs into cynomolgus monkeys (*Macaca fascicularis*), to
532 evaluate the short- and long-term toxicity of IMRCs in primates. After 6 months, acute toxicity data
533 showed that all blood biochemistry and urinalysis markers remained in the normal range (Fig. 5g, h;
534 Supplementary information, Fig. S9a), indicating normal liver, kidney, heart, muscular, pancreatic and
535 overall metabolic functions. Moreover, no abnormalities were observed in the long-term toxicity tests
536 either, suggesting minimal xenogeneic rejection responses (Supplementary information, Fig. S9b; n =
537 18). These results indicated that IMRCs have a robust safety profile in vitro and in vivo, and could
538 potentially provide therapeutic treatments with good safety levels for clinical potential.

IMRC transfusion treats lung injury and fibrosis in a dose-dependent manner

To evaluate the therapeutic effects of IMRCs on lung injury and fibrosis, IMRCs were administered intravenously into a bleomycin-induced model of lung injury (Fig. 6a). IMRCs ameliorated the total body weight reduction in mice exposed to bleomycin (BLM)-induced lung injury, in a dose-dependent manner (Fig. 6b). Kaplan-Meier survival curves indicated that IMRC treatment prolonged the overall survival rates (BLM group 12.5% vs. 1×10^6 IMRCs 25%, 3×10^6 IMRCs 50%, 5×10^6 IMRCs 62.5% ($P < 0.01$)) and the median survival time (BLM group 11.5 d vs. 1×10^6 IMRCs 15.5 d, 3×10^6 IMRCs 18.0 d, 5×10^6 IMRCs 21.0 d) in mice exposed to bleomycin-induced lung injury. There was a statistically significant difference between the BLM group and the 5×10^6 IMRCs group, but not the other groups (Fig. 6c). Histological staining of the lung at day 21 after bleomycin injection (inflammation phase) showed diffuse pneumonic lesions with loss of the normal alveolar architecture, septal thickening, enlarged alveoli, and increased infiltration of inflammatory cells in the interstitial and peribronchiolar areas, in the BLM lung compared with normal lung. IMRC treatment reduced alveolar thickening in the lung in a dose-dependent manner (Fig. 6d-f). Moreover, IMRC treatment reduced the number of macrophages in the lung (Fig. 6f). These results indicated that IMRC treatment can reduce inflammation in the lung after acute injury. Moreover, IMRC treatment also improved the Ashcroft score for pulmonary fibrosis in a dose-dependent manner (Fig. 6g). In particularly, IMRC treatment decreased collagen deposition in the BLM lung in a dose-dependent manner (Supplementary information, Fig. S10b, f). The expression levels of COL I, FN and α-SMA were also significant lower after IMRC treatment (Supplementary information, Fig. S10). ELISA showed that IMRC treatment reduced both TNF-α and TGF-β1 levels in the BLM lung in a dose-dependent manner (Fig. 6h, i). These results suggested that IMRCs can significantly reduce inflammation and fibrosis after lung injury, in a dose-dependent manner.

IMRC treatment of lung injury and fibrosis is superior to UCMSCs and pirfenidone injections

Pirfenidone (PFD) is an FDA-approved drug for the treatment of idiopathic pulmonary fibrosis. It works by reducing lung fibrosis through downregulating the production of growth factors and procollagens I and II. To evaluate the efficacy of IMRC treatment, we compared it side-by-side with UCMSCs and PFD treatments of BLM-injured mice (Fig. 6j). Our results showed that IMRC treatment

567 led to an improved amelioration of the weight reduction after BLM-induced lung injury, compared to
568 UCMSCs or PFD treatments (Fig. 6k). Kaplan-Meier survival curves indicated that the IMRC
569 treatments also resulted in the highest overall survival rates compared to UCMSCs or PFD treatments
570 (BLM group 39.02%, vs. IMRCs 70% ($P < 0.01$), UCMSCs 52.63%, PFD 65% ($P < 0.05$); Fig. 6l).
571 Moreover, IMRC treatment showed the best improvement in lung morphology (Supplementary
572 information, Fig. S11a) and the best reduction in BLM-induced edema, as measured by the lung
573 coefficient (lung wet weight/total body weight), compared to UCMSCs or PFD treatments
574 (Supplementary information, Fig. S11b).
575 Functionally, mice treated with IMRCs showed the best improvement in indices for lung capacity,
576 including pressure-volume (PV), inspiratory capacity (IC), static compliance (Crs) and forced vital
577 capacity (FVC) (Supplementary information, Fig. S12a-d). IMRC treatment also showed the best
578 reduction in functional indices for lung fibrosis, including respiratory resistance (Rrs), elastic resistance
579 (Ers), tissue damping (G) and tissue elasticity (H) were observed (Supplementary information, Fig.
580 S12e-h). Computed tomography (CT) scans also showed that IMRC treatment led to the best
581 improvement in lung morphology, compared to UCMSCs or PFD treatments (Supplementary
582 information, Fig. S12i, j). In fact, measurements of the lung volume indicated that mice treated with
583 IMRCs had the best improvement in lung volume compared to UCMSCs or PFD treatments. These
584 results indicated that the IMRC therapy is superior to primary UCMSCs and PDF in treating lung
585 injury and fibrosis.
586 Encouraged by these results, and in response to the urgency of the COVID-19 crisis in China, we
587 pilot-tested IMRC transfusion as compassionate treatments in two severely ill COVID-19 patients who
588 were diagnosed with ALI, as part of an expanded access program. After patient consent, IMRCs were
589 administered intravenously in both severely ill patients. Within 14 days after IMRC transfusion, both
590 the severely ill COVID-19 patients showed significant recovery from pneumonia, tested negative for
591 SARS-CoV-2, and were recommended for discharge. Cytokine analysis of both patients' plasma
592 showed very high levels of inflammatory cytokines initially in days 1-2, as expected of the
593 ALI-induced cytokine release syndrome that was manifesting at the point of treatment (Fig. 6m).
594 However, by days 4-8, many pro-inflammatory cytokines were suppressed after IMRC infusion,
595 including GRO-α, IFN-α2, IL-3, IL-9, IL-13, MCP-3, M-CSF, sCD40L and TNF-α (Fig. 6m). These
596 results suggested that IMRCs might possess a hyper-immunomodulatory function with potential

597 therapeutic benefits to ALI patients without other treatment options.

598 **Discussion**

599 In this study, IMRCs were derived from self-renewing hESC cultures with serum-free reagents. Our
600 results showed that IMRCs, while similar to primary UCMSCs, were superior in their long-term
601 proliferative capacity, hyper-immunomodulatory and anti-fibrotic functions. In addition, the cell
602 diameters of IMRCs were generally smaller than UCMSCs, suggesting that they pose lower risks for
603 pulmonary embolism after injection. Detailed analysis of mice and monkeys after IMRC injections
604 indicates that IMRCs do not engraft, nor transdifferentiate nor initiate tumorigenesis, showing excellent
605 potential for short- and long-term safety profiles by a range of in vitro and in vivo assays. Most
606 importantly, our experiments with the bleomycin mouse model of lung injury showed that treatments
607 with IMRCs are superior to primary UCMSCs and the FDA-approved pirfenidone in therapeutic
608 efficacy.
609 In recent years, MSC-like cells have been generated from hESCs using various protocols[18,19,36,37].
610 However, to the best of our knowledge and in spite of significant efforts by numerous groups,
611 previously reported studies lacked biosafety-related experiments. This has hindered their translation to
612 clinical application. To ensure safety, a series of biosafety-related experiments were performed
613 according to the "Guidelines for Human Somatic Cell Therapies and Quality Control of Cell-based
614 Products" and the IMRCs were verified as suitable for use in human therapy. Our data showed that
615 there was no teratoma formation observed after IMRC injection into the testes of NOD-SCID mice. In
616 addition, single cell RNA sequencing data showed no residual hESCs were detected in IMRCs and soft
617 agar assays also showed that no colonies were formed by IMRCs. In addition, the somatic mutation
618 analysis by whole genome sequencing also showed no mutations in proto-oncogenes and tumor
619 suppressor genes, nor any coding and non-coding exon regions of IMRCs. These results indicated that
620 IMRCs have no demonstrable potential to form tumors. Moreover, IMRCs could not undergo
621 long-term engraftment and disappeared around day 46. IMRCs did not transdifferentiate into
622 endothelial cells nor alveolar epithelial cells in the lung. To evaluate the risks of clinical application,
623 short- and long-term toxicity tests were performed in cynomolgus monkeys. After 6 months, both acute
624 toxicity tests and long-term toxicity test data showed that no abnormalities were observed. These

625 results proved that IMRCs could have an excellent safety profile and clinical potential. Moreover, the
626 above data suggested that the therapeutic efficacy of IMRCs may not be due to long-term engraftment
627 and direct repair of tissue, but due to their hyper-immunomodulatory and anti-fibrotic functions at
628 inflammatory sites of tissue interstitium.

629 Like MSCs, the IMRCs are immunoprivileged, and can escape allogeneic immune responses through
630 their lack of expression of HLA class II and their weak expression of HLA class I, thus making them
631 valuable choices for allogeneic cell therapy. Moreover, it has been reported that MSCs could release
632 immunomodulatory factors, alter the expression of surface molecules, and produce growth factors
633 during an immune response to the inflammatory cytokines produced by T cells and antigen-presenting
634 cells[38]. These immunomodulatory factors are crucial for regulating the immune system and promoting
635 tissue repair. Accordingly, expression of the T cell-suppressive *IDO1* greatly increased in IMRCs after
636 stimulation with the pro-inflammatory cytokine IFN-γ, even more than primary MSCs. Genome-wide
637 RNA sequencing revealed that IMRCs and UCMSCs had different expression profiles after exposure to
638 IFN-γ. Analysis of the secretomes of IMRCs and UCMSCs confirmed at least 9 pro-inflammatory
639 cytokines that were lower, and several anti-inflammatory cytokines and pro-regenerative factors that
640 were higher in IMRCs than UCMSCs. All these results suggested that IMRCs possess a
641 hyper-immunomodulatory capacity compared to primary UCMSCs, after stimulation with IFN-γ. Thus,
642 these cells can be administered to immunocompetent animals and human patients without the need for
643 further immunosuppression.

644 Moreover, higher levels of MMP1 were secreted by IMRCs than primary UCMSCs. MMP1 plays a
645 very important role in the process of fibrosis, by degrading existing collagens and promoting the early
646 stages of tissue remodeling that are critical for the progression of fibrogenesis[39,40]. In general, an
647 imbalance between MMPs and TIMPs is the direct cause of fibrosis and tissue scarring. It has been
648 reported that transplantation of human *MMP1*-overexpressing bone marrow-derived mesenchymal
649 stem cells can attenuate CCL4-induced liver fibrosis in rats[41]. Therefore, it is conceivable that IMRCs
650 that highly express MMP1 may also reverse lung fibrosis. Accordingly, our data showed that the
651 secretomes from IMRCs could reduce collagen I levels during fibrogenesis induced by TGF-β1.
652 However, it is still unclear whether MMP1 played a direct role in the decrease of collagen I. Future
653 work will focus on the role of MMP1 by using *MMP1*-knockout IMRCs in vitro and in vivo.

654 The mouse BLM model is similar to human ALI/ARDS during the acute inflammatory phase. Although

655 fibroblastic foci, alveolar epithelial type 2 cells hyperplasia and honeycombing lesions are reduced
656 compared with those in humans, indicating that the modeling of human ARDS is not complete in the
657 mouse BLM model, injury to alveolar epithelial cells has been shown to be a common contributing
658 factor to the pathogenesis of both human ARDS and BLM-induced mouse pulmonary injury[41,42]. To
659 test the therapeutic efficacy of IMRCs in the BLM mouse model, the delivery route and schedule of
660 administration (e.g. single dose versus repeated doses) were carefully considered. Intravenous infusion
661 is one of the principal delivery routes, considered to be minimally invasive, simple to use, and is the
662 most common mode for primary MSCs delivery in diverse lung disorders[43,44]. Furthermore, systemic
663 intravenous transplantation may be a suitable administration route in other future clinical scenarios. In
664 our present study, intravenous IMRCs improved the survival rate of mice with BLM-induced lung
665 injury in a dose-dependent manner, by inhibiting both pulmonary inflammation and fibrosis. As
666 demonstrated in vitro, IMRCs inhibited the production of pro-inflammatory cytokines and pro-fibrosis
667 cytokines, such as TNF-α and TGF-β1, in lung tissue in vivo. Furthermore, lung function indicators
668 such as PV, IC, Rrs, Crs, Ers, Rn, G, H and FVC were improved compared with the BLM group.
669 It should be noted that IMRCs were administered at 1 and 7 days after initiation of BLM-injury, but
670 before fibrosis has fully developed. In fact several studies have reported that primary MSCs treatments
671 do not improve pre-established pulmonary fibrosis, while some studies suggest that primary MSCs
672 actually exacerbate pulmonary fibrosis[45]. Regarding the efficacy of IMRCs in established fibrosis,
673 further studies are necessary and our own investigation is still ongoing. It is unclear whether primary
674 MSCs do promote pulmonary fibrosis, but their lack of positive therapeutic effect may be due to
675 differences in MSC subtypes and functions, fibrosis stages after induction, species of model animals,
676 and routes of administration of MSCs. Thus, clinical applications with MSCs should be considered
677 carefully. As noted in this study, it is important to carefully document the origin, preparation and
678 characterization of MSC-like cells. Here we have established a substantial profile of efficacy and safety
679 for the hESC-derived IMRCs. These efforts provide considerable grounds for hope that this artificial
680 cell-type could provide significant clinical benefit in the treatment of inflammatory and fibrotic disease
681 conditions.

682 **Conclusions**

In summary, our findings show that intravenously delivered IMRCs inhibited both pulmonary inflammation and fibrosis after acute lung injury in vivo. IMRCs significantly improved the survival rate in a dose-dependent manner. Furthermore, the mechanism for amelioration of pulmonary injury may be mediated by the IMRCs' paracrine action rather than their potential to differentiate and replace the damaged alveolar epithelial cells. The IMRCs' functional inhibition of TGF-β1-induced fibrosis could also be part of its mechanism. IMRCs were superior to UCMSCs and pirfenidone in therapeutic efficacy against lung injury and fibrosis. Furthermore, IMRCs showed an excellent safety profile in both mice and monkeys. In light of recent public health crises involving pneumonia, respiratory failure, ALI and ARDS, our pre-clinical results indicate that IMRCs are ready to be carefully considered for human trials in the treatment of lung injury and fibrosis.

Acknowledgements

This work was supported by Beijing Municipal Science & Technology Commission (Z181100003818005 to Qi Zhou), National Key Research and Development Program (2018YFA0108400 and 2017YFA0104403 to Jie Hao, 2017YFA0105001 and 2016YFA0101502 to Liu Wang, 2020YFC0843900 to Qi Zhou, 2020YFC0841900 to Baoyang Hu), the Strategic Priority Research Program of the Chinese Academy of Sciences (XDA16030701 to Liu Wang, XDA16030401 to Wei Li, XDA16040502 to Jie Hao), the National Natural Science Foundation of China (31621004 to Qi Zhou and Wei Li), the Key Research Projects of the Frontier Science of the Chinese Academy of Sciences (QYZDY-SSW-SMC002 to Qi Zhou), and China Postdoctoral Science Foundation (2019M660791 to Lei Wang).

Author contributions

B.H., H.D. and J.H. conceived the project and supervised the experiments. These authors contributed equally: J.W., D.S., Z.L. and B.G.. J.W., D.S., Z.L. and B.G. wrote the manuscript with help from all the authors. J.W., D.S., Z.L., B.G., Y.X., W.L., L.L., C.F., T.G., Y.C., Y.L., Z.W., J.W., S.Y., P.L., L.W., Y.W., L.P., H.W., T.Z., G.N.S., Z.H., G.F., W.L., Y.H., R.J., N.SC., Q.Z., L.W., B.H., H.D. and J.H. participated in the experiments and data analysis.

Competing interests

710 The authors declare no conflict of interest.

711 **References**

712 1. Yang, J. & Jia, Z. Cell-based therapy in lung regenerative medicine. *Regenerative medicine*
713 *research.* **2**, 7 (2014).
714 2. Fan, E., Brodie, D. & Slutsky, A. S. Acute Respiratory Distress Syndrome: Advances in
715 Diagnosis and Treatment. *Jama.* **319**, 698-710 (2018).
716 3. Rubenfeld, G. D. *et al.* Incidence and outcomes of acute lung injury. *N Engl J Med.* **353**,
717 1685-1693 (2005).
718 4. Bellani, G. *et al.* Epidemiology, Patterns of Care, and Mortality for Patients With Acute
719 Respiratory Distress Syndrome in Intensive Care Units in 50 Countries. *Jama.* **315**,
720 788-800 (2016).
721 5. Hamacher, J. *et al.* Tumor necrosis factor-alpha and angiostatin are mediators of endothelial
722 cytotoxicity in bronchoalveolar lavages of patients with acute respiratory distress
723 syndrome. *Am J Respir Crit Care Med.* **166**, 651-656 (2002).
724 6. Raghu, G. *et al.* An official ATS/ERS/JRS/ALAT statement: idiopathic pulmonary fibrosis:
725 evidence-based guidelines for diagnosis and management. *Am J Respir Crit Care Med.*
726 **183**, 788-824 (2011).
727 7. Marshall, R., Bellingan, G. & Laurent, G. The acute respiratory distress syndrome: fibrosis in
728 the fast lane. *Thorax.* **53**, 815-817 (1998).
729 8. Dhainaut, J. F., Charpentier, J. & Chiche, J. D. Transforming growth factor-beta: a mediator of
730 cell regulation in acute respiratory distress syndrome. *Critical care medicine.* **31**,
731 S258-264 (2003).
732 9. King, T. E., Jr. *et al.* A phase 3 trial of pirfenidone in patients with idiopathic pulmonary fibrosis.
733 *N Engl J Med.* **370**, 2083-2092 (2014).
734 10. Yoon, H. Y., Park, S., Kim, D. S. & Song, J. W. Efficacy and safety of nintedanib in advanced
735 idiopathic pulmonary fibrosis. *Respiratory research.* **19**, 203 (2018).
736 11. Zhou, H., Liu, M. & Lyu, X. [Research progress of mesenchymal stem cells in the treatment of
737 ALI]. *Zhonghua wei zhong bing ji jiu yi xue.* **29**, 1039-1042 (2017).
738 12. Serrano-Mollar, A. Cell Therapy in Idiopathic Pulmonary Fibrosis(†). *Med Sci (Basel).* **6**, 64
739 (2018).
740 13. Ortiz, L. A. *et al.* Interleukin 1 receptor antagonist mediates the antiinflammatory and
741 antifibrotic effect of mesenchymal stem cells during lung injury. *Proceedings of the*
742 *National Academy of Sciences of the United States of America.* **104**, 11002-11007
743 (2007).
744 14. Walter, J., Ware, L. B. & Matthay, M. A. Mesenchymal stem cells: mechanisms of potential
745 therapeutic benefit in ARDS and sepsis. *Lancet Respir Med.* **2**, 1016-1026 (2014).
746 15. G, W. J. *et al.* Mesenchymal stem (stromal) cells for treatment of ARDS: a phase 1 clinical trial.
747 *The Lancet. Respiratory medicine.* **3** (2015).
748 16. Thomson, J. A. *et al.* Embryonic stem cell lines derived from human blastocysts. *Science*
749 *(New York, N.Y.).* **282**, 1145-1147 (1998).
750 17. Barberi, T., Willis, L. M., Socci, N. D. & Studer, L. Derivation of multipotent mesenchymal
751 precursors from human embryonic stem cells. *PLoS medicine.* **2**, e161 (2005).

18. Hwang, N. S. *et al.* In vivo commitment and functional tissue regeneration using human embryonic stem cell-derived mesenchymal cells. *Proceedings of the National Academy of Sciences of the United States of America.* **105**, 20641-20646 (2008).
19. Vodyanik, M. A. *et al.* A mesoderm-derived precursor for mesenchymal stem and endothelial cells. *Cell stem cell.* **7**, 718-729 (2010).
20. Gu, Q. *et al.* Accreditation of Biosafe Clinical-Grade Human Embryonic Stem Cells According to Chinese Regulations. *Stem cell reports.* **9**, 366-380 (2017).
21. Pittenger, M. F. *et al.* Multilineage potential of adult human mesenchymal stem cells. *Science (New York, N.Y.).* **284**, 143-147 (1999).
22. Pittenger, M. F. *et al.* Mesenchymal stem cell perspective: cell biology to clinical progress. *NPJ Regenerative medicine.* **4**, 22 (2019).
23. Han, X. *et al.* Mapping human pluripotent stem cell differentiation pathways using high throughput single-cell RNA-sequencing. *Genome biology.* **19**, 47 (2018).
24. Kim, D., Langmead, B. & Salzberg, S. L. HISAT: a fast spliced aligner with low memory requirements. *Nature methods.* **12**, 357-360 (2015).
25. Trapnell, C. *et al.* Transcript assembly and quantification by RNA-Seq reveals unannotated transcripts and isoform switching during cell differentiation. *Nature biotechnology.* **28**, 511-515 (2010).
26. Huang da, W., Sherman, B. T. & Lempicki, R. A. Systematic and integrative analysis of large gene lists using DAVID bioinformatics resources. *Nature protocols.* **4**, 44-57 (2009).
27. Subramanian, A. *et al.* Gene set enrichment analysis: a knowledge-based approach for interpreting genome-wide expression profiles. *Proceedings of the National Academy of Sciences of the United States of America.* **102**, 15545-15550 (2005).
28. Prasad, V. K. *et al.* Efficacy and safety of ex vivo cultured adult human mesenchymal stem cells (Prochymal) in pediatric patients with severe refractory acute graft-versus-host disease in a compassionate use study. *Biology of blood and marrow transplantation : journal of the American Society for Blood and Marrow Transplantation.* **17**, 534-541 (2011).
29. Horibata, S., Vo, T. V., Subramanian, V., Thompson, P. R. & Coonrod, S. A. Utilization of the Soft Agar Colony Formation Assay to Identify Inhibitors of Tumorigenicity in Breast Cancer Cells. *Journal of visualized experiments : JoVE*, e52727 (2015).
30. Zhang, W. *et al.* SIRT6 deficiency results in developmental retardation in cynomolgus monkeys. *Nature.* **560**, 661-665 (2018).
31. Quinlan, A. R. & Hall, I. M. BEDTools: a flexible suite of utilities for comparing genomic features. *Bioinformatics (Oxford, England).* **26**, 841-842 (2010).
32. Berninger, M. T. *et al.* Fluorescence molecular tomography of DiR-labeled mesenchymal stem cell implants for osteochondral defect repair in rabbit knees. *European radiology.* **27**, 1105-1113 (2017).
33. Yang, J. *et al.* Tumor tropism of intravenously injected human-induced pluripotent stem cell-derived neural stem cells and their gene therapy application in a metastatic breast cancer model. *Stem cells (Dayton, Ohio).* **30**, 1021-1029 (2012).
34. Wagers, S., Lundblad, L., Moriya, H. T., Bates, J. H. & Irvin, C. G. Nonlinearity of respiratory mechanics during bronchoconstriction in mice with airway inflammation. *Journal of applied physiology (Bethesda, Md. : 1985).* **92**, 1802-1807 (2002).

35. Overmyer, K. A., Thonusin, C., Qi, N. R., Burant, C. F. & Evans, C. R. Impact of anesthesia and euthanasia on metabolomics of mammalian tissues: studies in a C57BL/6J mouse model. *PloS one.* **10**, e0117232 (2015).
36. Lian, Q. *et al.* Derivation of clinically compliant MSCs from CD105+, CD24- differentiated human ESCs. *Stem cells (Dayton, Ohio).* **25**, 425-436 (2007).
37. Lee, E. J. *et al.* Novel embryoid body-based method to derive mesenchymal stem cells from human embryonic stem cells. *Tissue engineering. Part A.* **16**, 705-715 (2010).
38. Shi, Y. *et al.* How mesenchymal stem cells interact with tissue immune responses. *Trends in immunology.* **33**, 136-143 (2012).
39. Milani, S. *et al.* Differential expression of matrix-metalloproteinase-1 and -2 genes in normal and fibrotic human liver. *The American journal of pathology.* **144**, 528-537 (1994).
40. Benyon, R. C., Iredale, J. P., Goddard, S., Winwood, P. J. & Arthur, M. J. Expression of tissue inhibitor of metalloproteinases 1 and 2 is increased in fibrotic human liver. *Gastroenterology.* **110**, 821-831 (1996).
41. Du, C. *et al.* Transplantation of human matrix metalloproteinase-1 gene-modified bone marrow-derived mesenchymal stem cell attenuates CCL4-induced liver fibrosis in rats. *International journal of molecular medicine.* **41**, 3175-3184 (2018).
42. Sgalla, G. *et al.* Idiopathic pulmonary fibrosis: pathogenesis and management. *Respiratory research.* **19**, 32 (2018).
43. Zhu, Y. G., Hao, Q., Monsel, A., Feng, X. M. & Lee, J. W. Adult stem cells for acute lung injury: remaining questions and concerns. *Respirology (Carlton, Vic.).* **18**, 744-756 (2013).
44. Kanelidis, A. J., Premer, C., Lopez, J., Balkan, W. & Hare, J. M. Route of Delivery Modulates the Efficacy of Mesenchymal Stem Cell Therapy for Myocardial Infarction: A Meta-Analysis of Preclinical Studies and Clinical Trials. *Circulation research.* **120**, 1139-1150 (2017).
45. Weiss, D. J. & Ortiz, L. A. Cell therapy trials for lung diseases: progress and cautions. *Am J Respir Crit Care Med.* **188**, 123-125 (2013).

Figure legends

Figure 1

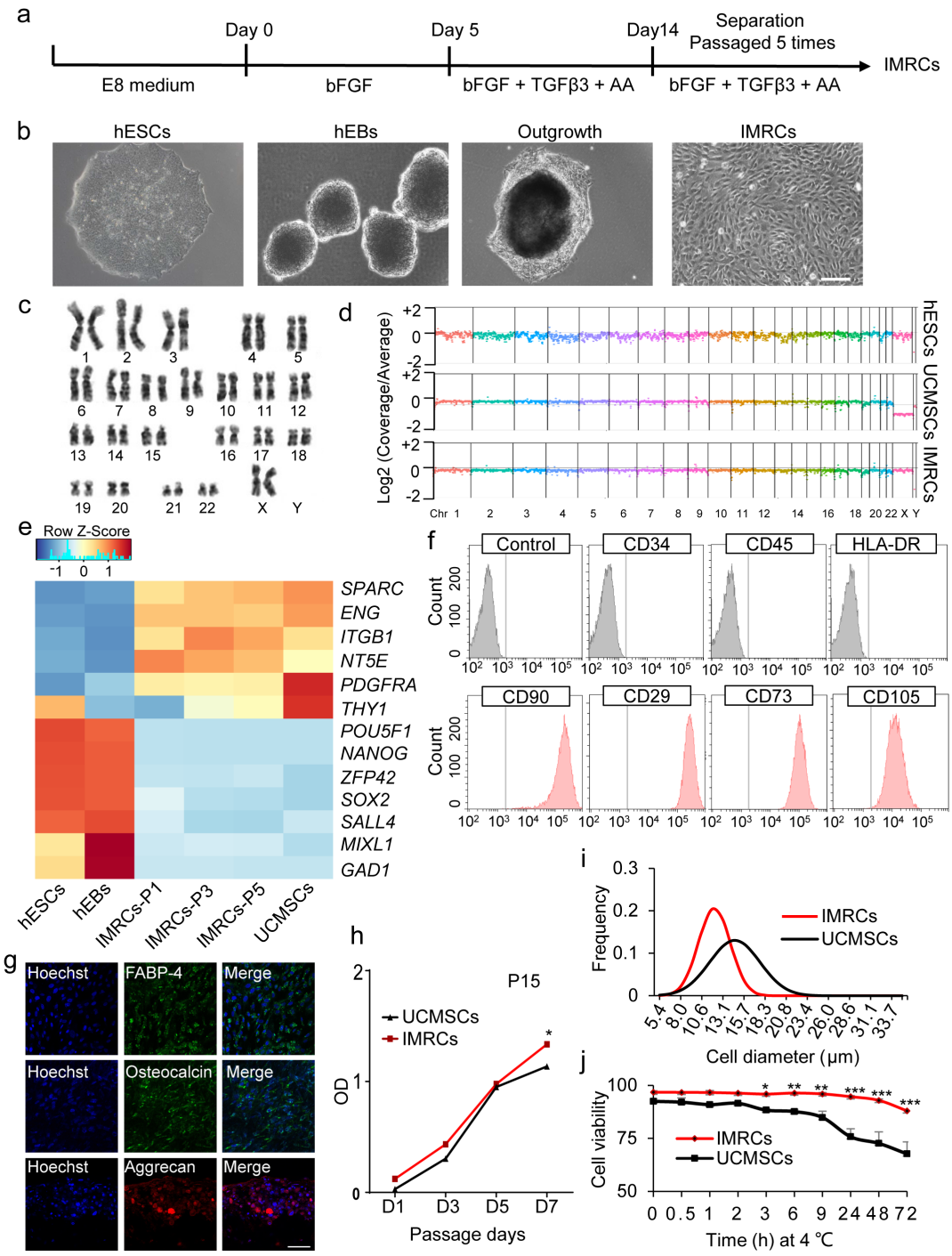

Fig. 1 Derivation of immunity- and matrix-regulatory cells (IMRCs) from human embryonic stem cells (hESCs).

a Different phase of the IMRCs derivation protocol. AA, L-ascorbic acid. **b** Representative morphology of cells at different stages as observed by phase contrast microscopy. hEBs, human embryoid bodies. Scale bars, 100 μm. **c** A representative chromosome spread of normal diploid IMRCs

836 with 22 pairs of autosomes and two X chromosomes. **d** Copy number variation (CNV) analysis by
837 whole genome sequencing for hESCs, primary UCMSCs and IMRCs. UCMSCs, umbilical cord
838 mesenchymal stem cells. **e** Heatmap showing MSC-specific marker and pluripotency marker gene
839 expression changes, from hESCs and hEBs to IMRCs at passages 1-5 (P1-5), and primary UCMSCs. **f**
840 IMRCs' expression of MSC-specific surface markers was determined by flow cytometry. Isotype
841 control antibodies were used as controls for gating. Like MSCs, the IMRCs are
842 $CD34^-/CD45^-/HLA\text{-}DR^-/CD90^+/CD29^+/CD73^+/CD105^+$ cells. **g** Representative immunofluorescence
843 staining of IMRCs after they were induced to undergo adipogenic differentiation (FABP-4), osteogenic
844 differentiation (Osteocalcin), and chondrogenic differentiation (Aggrecan). Scale bars, 100 μm. **h**
845 Proliferation curve of IMRCs and UCMSCs at the 15th passage (n = 5). **i** Distribution of cell diameters
846 of IMRCs and UCMSCs. **j** Viability of IMRCs and UCMSCs in clinical injection buffer over time at
847 4 °C. * $p < 0.05$, ** $p < 0.01$, *** $p < 0.001$; data are represented as the mean ± SEM.

Figure 2

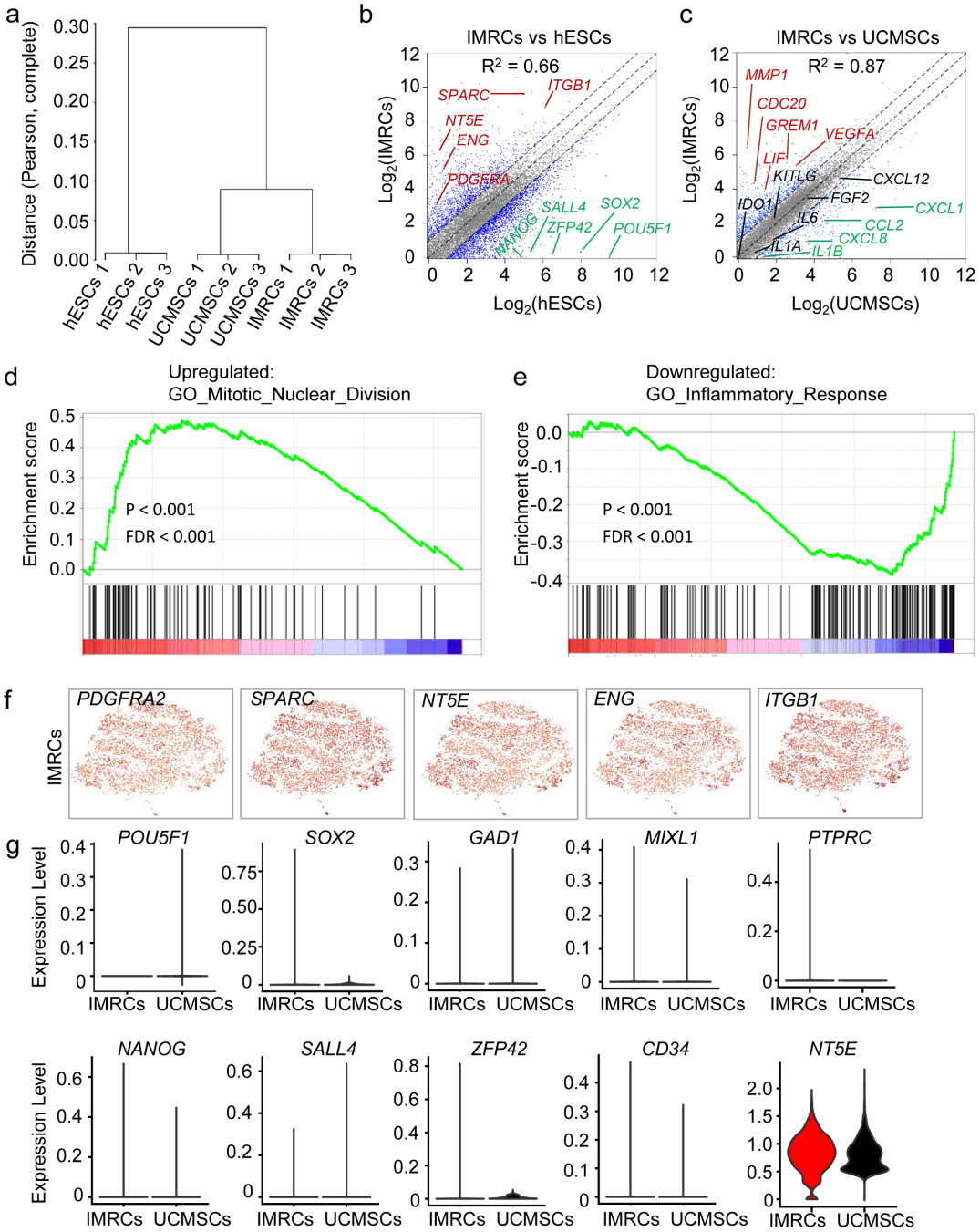

Fig. 2 IMRCs possess unique gene expression characteristics.

a Unsupervised hierarchical clustering analysis based on the Pearson correlation distance between the whole mRNA profile of each cell type. **b** Scatter plot displaying the differentially expressed genes (DEGs) between IMRCs and hESCs. Up-regulated genes are highlighted in red. Down-regulated genes are highlighted in green. Gray dots represent non-DEGs (< 2-fold change). **c** Scatter plot displaying the DEGs between IMRCs and primary UCMSCs. Up-regulated genes are highlighted in red.

Down-regulated genes are highlighted in green. Gray dots represent non-DEGs (< 2-fold change). **d** Gene set enrichment analysis (GSEA) of the top up-regulated gene signature in IMRCs, compared with primary UCMSCs. **e** GSEA of the top down-regulated gene signature in IMRCs, compared with UCMSCs. **f** Heatmaps of specific gene expression amongst single IMRCs groups. **g** Quantification of non-mesenchymal marker gene expression amongst single IMRCs, UCMSCs and hESCs, as measured by single cell RNAseq.

Figure 3

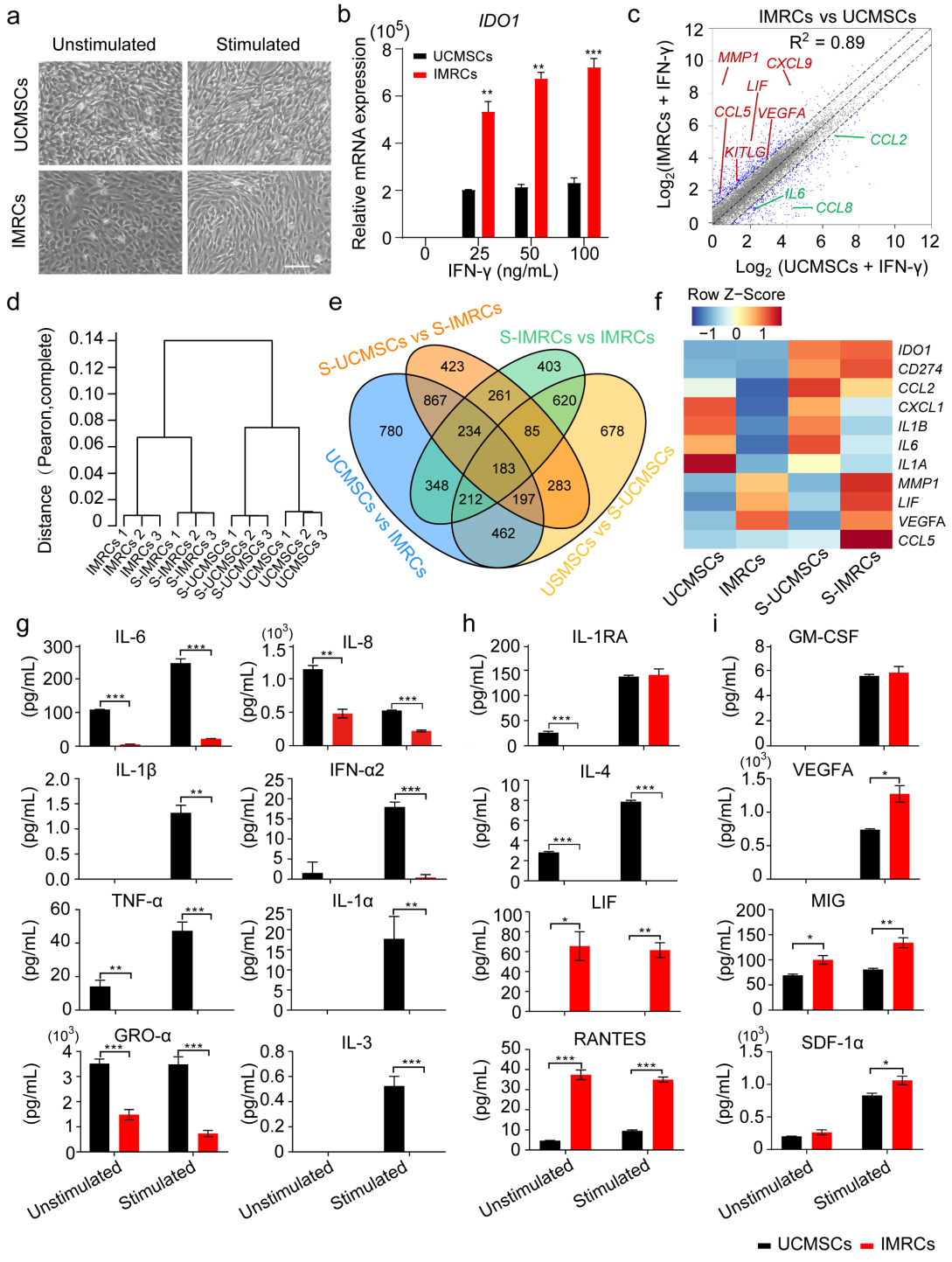

862 **Fig. 3 IMRCs activated by IFN-γ show hyper-immunomodulatory potency.**

863 **a** Morphology of UCMSCs and IMRCs before and after IFN-γ (100 ng/mL) stimulation. **b** Quantitative
864 PCR for *IDO1* mRNA in UCMSCs and IMRCs before and after IFN-γ (0, 25, 50, 100 ng/mL)
865 treatment. *GAPDH* was used for internal normalization. **c** Scatter plot displaying the DEGs between
866 UCMSCs and IMRCs after treatment with 100 ng/mL IFN-γ. Up-regulated genes are highlighted in red.
867 Down-regulated genes are highlighted in green. Gray dots represent non-DEGs (< 2-fold change). **d**
868 Unsupervised hierarchical clustering analysis of UCMSCs and IMRCs, before and after IFN-γ
869 stimulation (S-UCMSCs and S-IMRCs). **e** Venn diagram shows the overlap among UCMSC- and
870 IMRCs-associated genes, before and after IFN-γ stimulation (S). **f** Heatmap illustrating the expression
871 of cytokines in UCMSCs and IMRCs, before and after IFN-γ stimulation (S). **g-i** ELISA analysis of
872 biologically relevant chemokines and cytokines in the secretomes of unstimulated or stimulated IMRCs
873 and UCMSCs. Pro-inflammatory (G), immunomodulatory (H), and pro-regenerative (I) cytokines. * p
874 < 0.05, ** $p < 0.01$, *** $p < 0.001$; data are represented as the mean ± SEM. Scale bar, 100 μm.

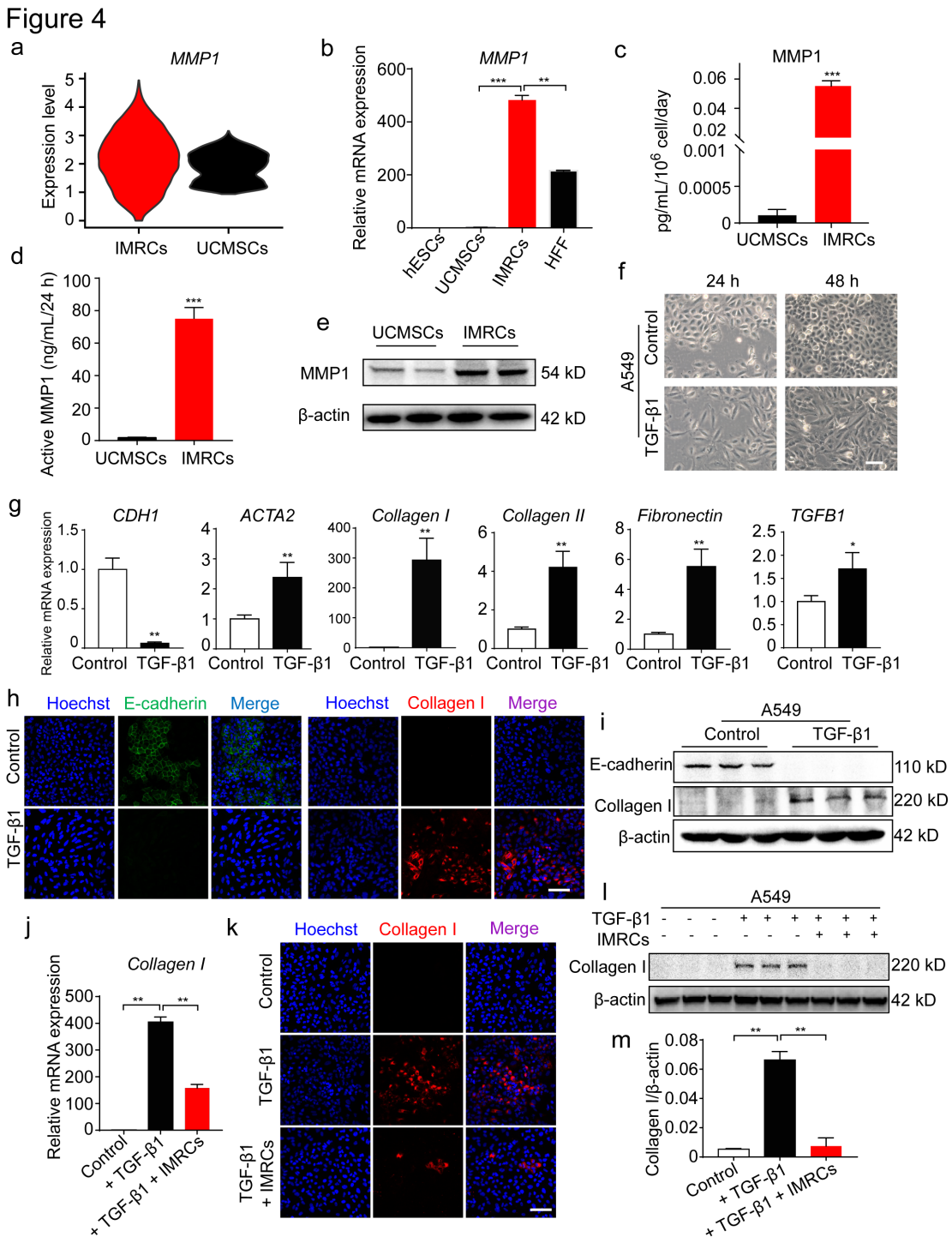

Fig. 4 IMRCs reduce the pro-fibrotic effects of TGF-β1.

a Quantification of *MMP1* gene expression amongst single IMRCs, UCMSCs and hESCs, as measured by single cell RNAseq. **b** Quantitative PCR for *MMP1* mRNA in hESCs, UCMSCs, IMRCs and human foreskin fibroblasts (HFF). **c** ELISA for MMP1 protein in the conditioned media of IMRCs and UCMSCs. **d** MMP1 activity in the conditioned media of IMRCs and UCMSCs. **e** Western blot for MMP1 protein in IMRCs and UCMSCs. β-actin was used as a loading control. **f** Representative

882 morphology of A549 cells, with or without 10 ng/mL TGF-β1 treatment for 48 h. **g** Quantitative PCR
883 for the relative expression of *CDH1*, *ACTA2*, *Collagen I*, *Collagen II, Fibronectin* and *TGFB1* mRNA
884 in A549 cells, with or without TGF-β1 treatment for 48 h. **h** Immunofluorescence staining for
885 E-cadherin and Collagen I expression in A549 cells, with or without 10 ng/mL TGF-β1 treatment for
886 48 h. **i** Western blot for E-cadherin and Collagen I protein expression in A549 cells, with or without 10
887 ng/mL TGF-β1 treatment for 48h. **j** Quantitative PCR for *Collagen I* mRNA in A549 cells, with or
888 without 10 ng/mL TGF-β1 and IMRC conditioned media treatment for 48 h. **k** Immunofluorescence
889 staining for E-cadherin and Collagen I expression in A549 cells, with or without 10 ng/mL TGF-β1 and
890 IMRC conditioned media treatment for 48 h. **l** Western blot for E-cadherin and Collagen I protein
891 expression in A549 cells, with or without 10 ng/mL TGF-β1 and IMRC conditioned media treatment
892 for 48 h. **m** Quantification of the relative Collagen I protein expression levels in **(l)**. * $p < 0.05$, ** $p <$
893 0.01, *** $p < 0.001$; data are represented as the mean ± SEM. Scale bar, 100 μm.

Figure 5

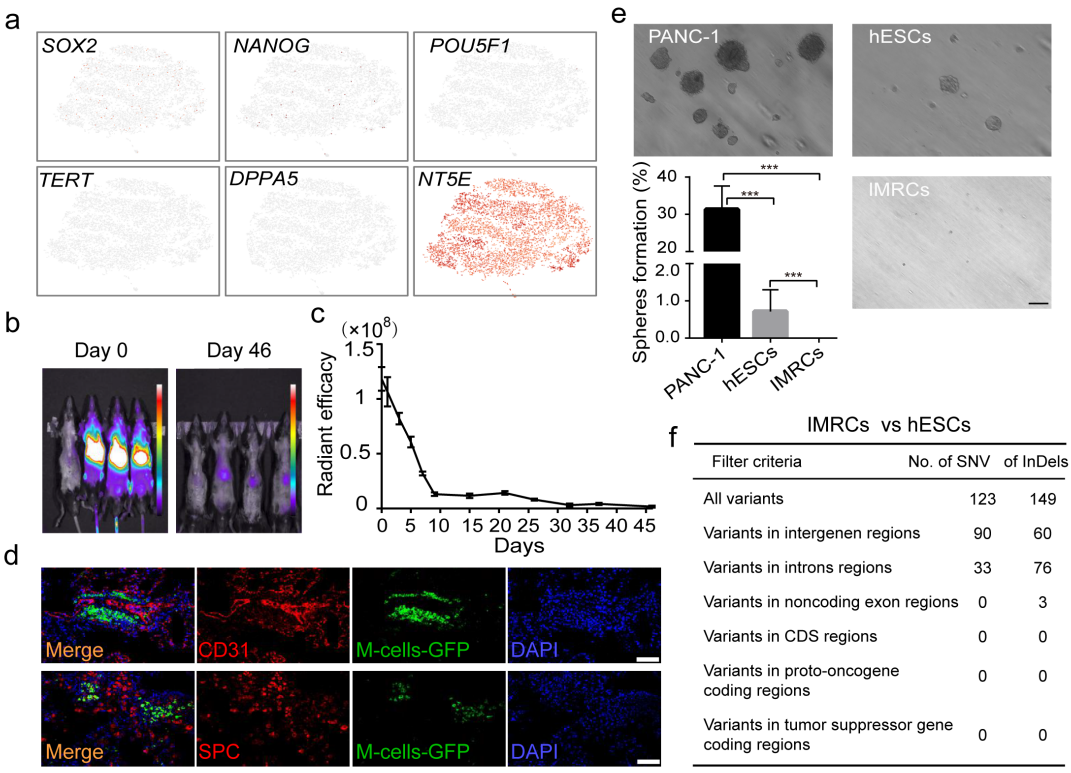

f

IMRCs vs hESCs

Filter criteria	No. of SNV	of InDels
All variants	123	149
Variants in intergenen regions	90	60
Variants in introns regions	33	76
Variants in noncoding exon regions	0	3
Variants in CDS regions	0	0
Variants in proto-oncogene coding regions	0	0
Variants in tumor suppressor gene coding regions	0	0

g Acute toxicity test in cynomolgus monkeys: blood biochemistry (after 6 months)

Group	ALT (U/L)	AST (U/L)	ALP (U/L)	CK (U/L)	GGT (U/L)	LDH (U/L)	TBIL (μmol/L)	BUN (mmol/L)	CRE (μmol/L)	GLU (mmol/L)	CHO (mmol/L)	TG (mmol/L)
1×10^8	55.00	30.00	165.00	123.00	65.00	497.00	3.00	6.00	58.00	5.00	3.00	1.00
0.26×10^8	73.00	34.00	160.00	164.00	38.54	330.00	3.17	8.00	61.00	4.05	3.83	0.32
0.026×10^8	63.00	49.00	94.00	317.00	51.64	298.00	5.89	7.60	71.00	2.57	2.60	0.32

Group	TP (g/L)	ALB (g/L)	A/G	IgA (g/L)	IgG (g/L)	IgM (g/L)	C3 (g/L)	C4 (g/L)	K^+ (mmol/L)	Na^+ (mmol/L)	Cl^- (mmol/L)
1×10^8	71.00	42.00	1.00	1.00	6.00	1.00	1.00	0.00	3.00	146.00	108.00
0.26×10^8	72.20	42.60	1.44	1.79	7.48	0.76	0.93	0.14	3.62	145.4	98.00
0.026×10^8	78.70	40.90	1.08	2.81	10.81	0.73	0.96	0.09	3.45	146.8	99.80

h Acute toxicity test in cynomolgus monkeys: urinalysis (after 6 months)

Group	GLU (mmol/L)	PRO (mg/L)	BIL (μmol/L)	URO (μmol/L)	PH	SG	ERY (mg/L)	KET (mmol/L)	NIT	Color
1×10^8	-	-	-	Normal	8.5	< 1.005	-	-	-	Light yellow
0.26×10^8	-	+-	-	Normal	8.5	1.015	-	-	-	Yellow
0.026×10^8	-	-	-	Normal	8.0	1.015	-	-	1 +	Colorless

Fig. 5 Evaluation of the safety of IMRC transfusion.

a t-SNE projection of single cells and their pluripotency gene expression amongst IMRCs. **b** In vivo imaging of the far red fluorescence in mice after injection of DiR-labeled IMRCs. **c** Quantification of the DiR fluorescent radiance in the whole body over time. **d** Immunofluorescence staining of lung sections for the endothelial marker CD31 and the alveolar epithelial marker SPC, 21 days after injecting GFP-labeled IMRCs. Scale bar, 100 μm. **e** Soft agar colony formation assay for the

901 tumorigenic potential of IMRCs, relative to PANC-1 cancer cells and hESCs. Scale bar, 100 μm. **f**
902 Single nucleotide variants (SNVs) and insertions/deletions (InDels) in the non-repeat regions of the
903 IMRCs genome, relative to hESCs. **g** Blood biochemistry results of cynomolgus monkeys (*Macaca*
904 *fascicularis*) injected with a low (2.6×10^6), medium (2.6×10^7) or high (1×10^8) dose of IMRCs after
905 six months. AST, aspartate aminotransferase; ALT, alanine aminotransferase; ALP, alkaline
906 phosphatase; CK, creatine phosphokinase; GGT, glutamyltransferase; LDH, lactate dehydrogenase;
907 TBIL, total bilirubin; BUN, urea nitrogen; CRE, creatinine; GLU, glucose; CHO, total cholesterol; TG,
908 triglyceride; TP, total protein; ALB, albumin; A/G, albumin/globulin. **h** Urinalysis results of
909 cynomolgus monkeys (*Macaca fascicularis*) injected with a low (2.6×10^6), medium (2.6×10^7) or
910 high (1×10^8) dose of IMRCs after six months. PRO, urine protein; BIL, urine bilirubin; URO, urinary
911 gallbladder; pH, acid degree value; SG, specific gravity; ERY, erythrocyte; KET, ketone; NIT, nitrite. *
912 $p < 0.05$, ** $p < 0.01$, *** $p < 0.001$; data are represented as the mean ± SEM.

Figure 6

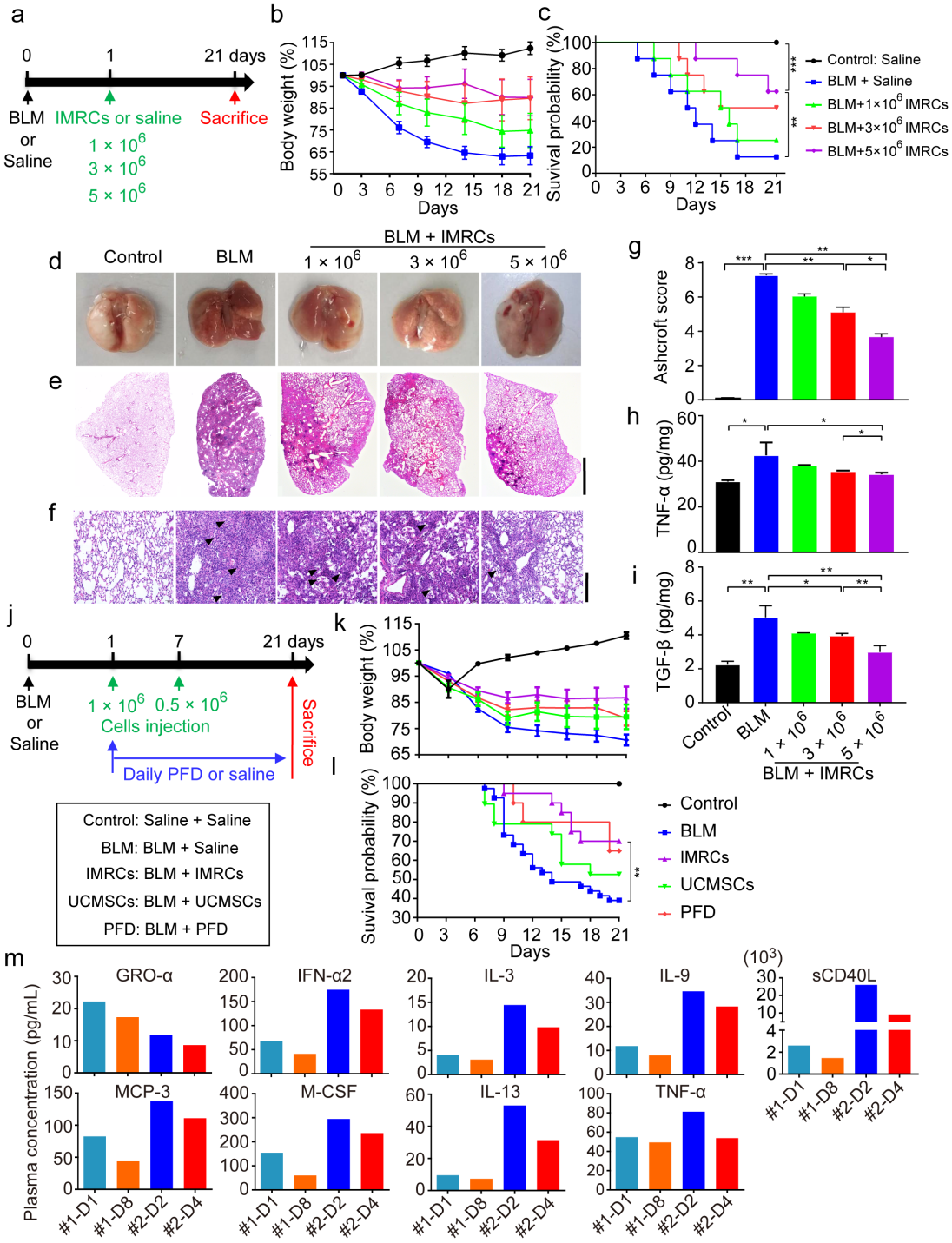

Fig. 6 IMRC transfusion treats lung injury and fibrosis dose-dependently.

a Diagram of the animal experimental protocol for dose escalation. Mice received intratracheal bleomycin (BLM; 2.5 mg/kg body weight) or the same amount of saline at day 0. At day 1, some BLM-injured mice received an intravenous (I.V.) injection of 1×10^6, 3×10^6 or 5×10^6 IMRCs via the caudal vein. A group of BLM-injured mice and normal control mice received the same volume of saline. Mice were randomly grouped (n = 8 per group). **b** Relative body weight (%) changes of the

920 mice receiving different interventions. **c** Kaplan-Meier survival curves of the mice receiving different
921 interventions. **d** Representative images of whole lung from all groups at day 21 post-injury. **e, f**
922 Representative histology of lung sections stained with H&E (Scale bar, 2 mm and 200 μm) at 21 days
923 post-injury. Arrowheads, inflammatory infiltration. **g** Quantitative evaluation of fibrotic changes with
924 the Ashcroft score in lungs of mice receiving different interventions. The Ashcroft scores based on the
925 lung H&E sections. The severity of fibrotic changes in each section was assessed as the mean score of
926 severity in the observed microscopic fields. Six fields per section were analyzed. **h, i** ELISA for the
927 protein levels of TNF-α and TGF-β1 in the lungs of mice receiving different interventions. **j** Diagram
928 of the animal experimental protocol for multiple arm testing. Double I.V. injections of 1×10^6 and 0.5
929 $\times 10^6$ IMRCs (at days 1 and 7 respectively) were compared side-by-side with double I.V. injections of 1
930 $\times 10^6$ and 0.5×10^6 UCMSCs (at days 1 and 7 respectively), vs. daily pirfenidone (PFD) or saline
931 treatments of mice injured with intratracheal bleomycin (BLM; 2.5 mg/kg body weight) at day 0. **k**
932 Relative body weight (%) changes of mice receiving different interventions. **l** Kaplan-Meier survival
933 curves of mice receiving different interventions. **m** ELISA analysis of pro-inflammatory cytokines in
934 the plasma of two ALI patients after intravenous IMRC transfusion. * $p < 0.05$, ** $p < 0.01$, *** $p <$
935 0.001; data are represented as the mean ± SEM.
936